Yields and molecular composition of gas phase and secondary organic aerosol from the photooxidation of the volatile consumer product benzyl alcohol: formation of highly oxygenated and hydroxy nitroaromatic compounds

Mohammed Jaoui[1], Kenneth S. Docherty[2], Michael Lewandowski[1], Tadeusz E. Kleindienst[1]

[1]Center for Environmental Measurement & Modeling, U.S. Environmental Protection Agency, Research Triangle Park, NC, 27711, USA
[2]Jacobs Technology, Inc., Research Triangle Park, NC, 27709, USA

Correspondence: Mohammed Jaoui (Jaoui.mohammed@epa.gov)
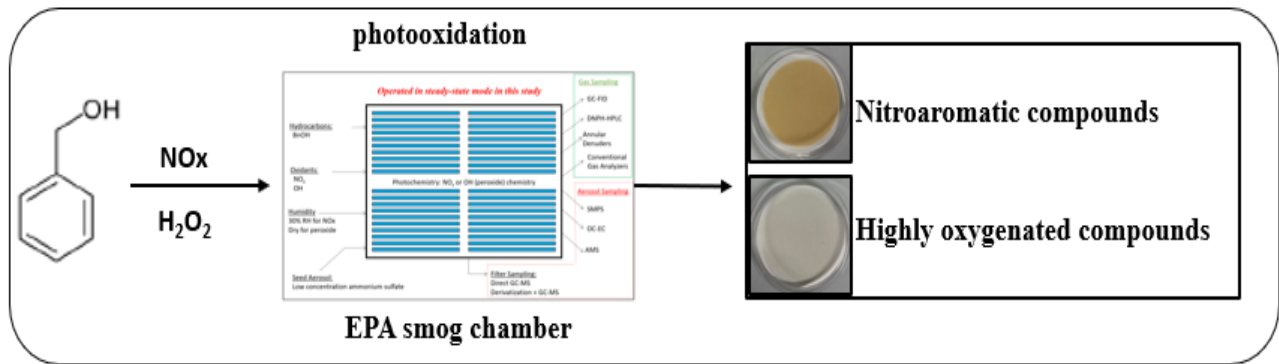
Abstract. Recently, volatile chemical products (VCPs) have been increasingly recognized as important precursors for secondary organic aerosol (SOA) and ozone in urban areas. However, their atmospheric chemistry, physical transformation, and their impact on climate, environment, and human health remain poorly understood. Here, the yields and chemical composition at the molecular level of gas and particle phase products originating from the photooxidation of one of these VCPs, benzyl alcohol (BnOH), are reported. The SOA was generated in the presence of seed aerosol from nebulized ammonium sulfate solution in a 14.5 m^3 smog chamber operated in flow mode. More than 50 organic compounds containing nitrogen and/or up to seven oxygen atoms were identified by mass spectrometry. While a detailed non-targeted analysis has been made, our primary focus has been to examine highly oxygenated and nitro-aromatic compounds. The major components include ring-opening products with high oxygen to carbon ratio (e.g., malic acid, tartaric acids, arabic acid, trihydroxy-oxo-pentanoic acids, and pentaric acid), and ring-retaining products (e.g., benzaldehyde, benzoic acid, catechol, 3-nitrobenzyl alcohol, 4-nitrocatechol, 2-hydroxy-5-nitrobenzyl alcohol, 2-nitrophloroglucinol, 3,4-dihydroxy-5-nitrobenzyl alcohol). The presence of some of these products in the gas and particle phases simultaneously provides evidence of their gas/particle partitioning. These oxygenated oxidation products made dominant contributions to the SOA particle composition in both low and high NOx systems. Yields, organic mass to organic carbon ratio, and proposed reaction schemes for selected compounds are provided. The aerosol yield was 5.2% for BnOH/H_2O_2 at SOA concentration of 52.9 µg m^{-3} and ranged between 1.7-8.1 % for BnOH/NOx at SOA concentration of 40.0-119.5 µg m^{-3}.

Key words: Benzyl alcohol, highly oxygenated compounds, Consumer products, VCPs, Silylation, Yield, Nitroaromatic compounds, SOA

1 Introduction

Modeling atmospheric organic aerosol (OA) using chemical transport models (CTMs) is complex, challenging, and often can lead to model-measurement discrepancies (Zhao et al., 2016). Applying CTMs to urban areas reveals that traditional VOCs including combustion-related processes cannot account for the observed OA mass, leaving a substantial fraction unresolved (Hayes et al., 2015). Recent studies suggest that this discrepancy is due in part to unaccounted, rapidly reacting SOA and ozone precursors from unknown sources (Hodzic et al, 2009; Hayes et al., 2015; McDonald et al., 2018; Akherati et al. 2019; Lu et al., 2020). Volatile chemical products (VCPs), such as personal care products, cleaning agents, coatings, adhesives, and pesticides have emerged as possible sources in urban areas (McDonald et al., 2018). Their emissions can be larger than those from usual sources, such as motor vehicles (Coggon et al., 2021). Laboratory, modeling, and field studies for VCPs have been conducted to assess their potential to affect ambient OA and ozone formation in urban and suburban locations (McDonald et al., 2018; Khare et al., 2018; Stockwell et al., 2021; Seltzer et al., 2021; Gkatzelis et al., 2021; Milani et al., 2021; Pennington et al., 2021; Coggon et al., 2021). The contribution of VCPs to ambient OA is not fully understood and only limited modeling studies have been reported (Mohr et al., 2015; Vlachou et al., 2018; Pennington et al., 2021; Qin et al., 2021; Seltzer et al., 2021). Additionally, few experimental and chamber studies of VCPs have been conducted with limited characterization of aerosol products (Wu and Johnston, 2016, 2017; Harrison and Well, 2012; Charan et al., 2020, 2021; Humes et al., 2022). For example, the analysis of SOA from the oxidation of cyclic methyl siloxanes (Wu and Johnston, 2016, 2017; Fu et al. 2020; Alton and Browne, 2020; Charan et al., 2021) and cyclic siloxanes (Janechek et al., 2019) has been conducted. Kinetic studies with limited products characterization have been reported for the oxidation of benzyl alcohol (BnOH) by hydroxyl radicals (Bernard et al., 2013; Wang, 2015; Harrison and Well, 2009, 2012). Recently, Humes et al. (2022) highlight the importance of oxygenated aromatic VCPs emission to generate urban SOA and oxygenated products in both gas and aerosol phases. Therefore, understanding the atmospheric chemistry of VCPs is important to assess their role in air quality and climate and to improve SOA chemistry in CTMs thereby allowing for better estimates in health studies and source apportionment.

The challenges associated with evaluating VCP impacts on urban OA can be addressed by identifying atmospheric VCP concentrations and SOA markers linking those VCP to ambient particulate matter (PM). Benzyl alcohol (C_7H_8O) is an important ring containing VCP used as an organic intermediate and a solvent in a wide range of applications (Antonelli et al. 2002). BnOH is emitted also from flowers and flowering trees (Do et al., 1969; Horvat et al., 1990; Larsen and Poll, 1990; Humpf and Scheier, 1991; Boatright et al., 2004; Vallat and Dorn, 2005; Orlova et al.; 2006) and found in indoor

77   air (Weschler, 2011). Gas kinetic studies of loss rates and product distributions have been conducted using flow tubes and

78   environmental chambers. Bernard et al. (2013) examined the rate and mechanisms of the OH + BnOH reaction. Similarly,

79   Harrison and Wells (2009, 2012) investigated the rate constants for the BnOH reaction with ozone, OH and NO_3 radicals.

80   Carter et al. (2005) conducted chamber experiments to assess ozone and PM formation from BnOH and related

81   compounds. Product studies from BnOH oxidation have focused mainly on gas phase (GP) products. Several carbonyl

82   products (benzaldehyde (BnAld), formaldehyde, glyoxal, butenedial, 4-oxopentanal, 3-hydroxy-2-propanaldehyde), and

83   benzyl nitrate, o-hydroxybenzyl alcohol, o-dihydroxy benzene were reported from the above studies. With respect to the

84   particle phase (PP), Charan et al. (2020) reported aerosol yields from BnOH oxidation together with a limited number of

85   SOA products. Finally, Wang (2015) conducted a theoretical study to elucidate the reaction mechanism of the oxidation

86   of BnOH with OH radicals.

87   In this study, we report a detailed non-targeted chemical analysis of GP and SOA products originated from the

88   photooxidation of BnOH in the presence and absence of oxides of nitrogen (NOx), with the aim to better understand the

89   chemical composition at the molecular level. Gas chromatography-mass spectrometry (GC-MS) and high-performance

90   liquid chromatography were used for the identification of a range of organic compounds including oxygenated

91   nitroaromatics and related compounds bearing up to seven oxygen atoms. Nitroaromatics are pollutants of concern due to

92   their toxicity, light-absorption properties, and relatively long residence times in the environment. Highly oxygenated

93   compounds can partition into pre-existing particles or be involved in new particle formation. Also, in the present study,

94   SOA and secondary organic carbon (SOC) yields were measured with the results compared to published data. A chemical

95   mechanism is then proposed to represent and account for selected gas- and aerosol-phase products observed in this study.

96

97   **2 Experimental methods**

98   All chemicals including N, O-*bis*(trimethylsilyl) trifluoroacetamide (BSTFA) derivatization reagent with 1%

99   trimethylchlorosilane (TMCS) as catalyst and benzyl alcohol (99%), 2-methyl-4-nitrophenol, L-(+)-tartaric acid, D-(-)-

100   tartaric acid, and meso-tartaric acid were purchased from Aldrich Chemical Co. (Milwaukee, WI) at the highest purity

101   (99.8%) available and were used without further purification. In addition to standards reported in our previous studies

102   (Jaoui et al., 2004; 2018), 3-nitrobenzyl alcohol, benzoic acid, and 4-nitrocatechol were purchased from Tokyo Chemical

103   Industry (OR, USA); while pentaric acid, 2,3-dihydroxy-4-methoxy-4-oxobutanoic acid, and arabic acid were obtained

104   from Aurum Pharmatech, LLC (NJ, USA).

2.1 Chamber description and operation

All experiments were conducted in a 14.5 m^3 fixed-volume chamber having TFE Teflon coated walls and maintained at a positive pressure of 0.1 Torr. The chamber operation, procedures, and instrumentation have been described previously (Kleindienst et al. 2006; 2009), and here just experiment-specific details are primarily included. A combination of fluorescent bulbs having radiation from 300-400 nm was used to photolyze NO_2. In the absence of NO_x, the radiation system was altered to include UV-313 sunlamps to adequately photolyze H_2O_2. The chamber was operated in steady-state (SS or flow) mode to provide continuously stable effluent concentrations. Under these conditions, reactants and products equilibrate with the chamber surfaces to minimize irreversible losses of gases and particles. The SS operation allows for extended sampling periods to improve the accuracy and precision of the measurements (Shilling et al., 2008). Temperature, relative humidity, and UV light intensity were measured continuously with an uncertainty of 5%. Pre-experiment and post-experiment procedures (see section 2.5 below) were routinely carried out before and after each experiment to minimize contamination in the chamber. The reactant generation system provided constant sources of zero air, reactants, water vapor, and ammonium sulfate (AS) seed aerosol. The reactant flow of gases (e.g., NO_x) into the chamber was regulated using mass flow controllers. BnOH was injected using a syringe pump, vaporized in a heated glass bulb, and injected with zero air. For experiments in the absence of NOx, a 50% aqueous solution of H_2O_2 was vaporized and injected using a second syringe pump, and photolyzed to produce OH radicals. Typical chamber AS concentrations were approximately 1 $\mu g\ m^{-3}$. Each SS experiment went through an initial transient period of 18-24 h until the reactant and product concentrations reached steady state.

2.2 Gas-phase measurements

A wide variety of instruments were used to measure the reactants and products. Nitric oxide (NO) and NOx were measured with a TECO (Franklin, MA) oxides of nitrogen analyzer with an upstream nylon filter to remove nitric acid produced from OH + NO_2. The NOx analyzer was calibrated with a NIST-traceable NO standard. Initial H_2O_2 concentrations were estimated by UV absorption using the ratio of the H_2O_2 to O_3 absorbances at 254 nm, as described by Kleindienst et al. (2009). Experiments in the absence of NOx were conducted dry to avoid aqueous loss of H_2O_2. BnOH concentrations in the inlet and within the chamber were measured semi-continuously using an SRI Model 8610C compact gas chromatograph with flame ionization detector (GC-FID; SRI Instruments, Torrance CA). The purity of the BnOH was verified with GC-MS analysis.

133   Low molecular weight carbonyls and dicarbonyls were quantified by derivatization using 2,4-dinitrophenylhydrazine

134   (Smith et al., 1989). Samples were collected at 0.5 L min^{-1} for 25 min and derivatized in a 4 mL solution of acidified

135   DNPH and then heated for 40 min at 70°C. Air samples were drawn for 20 min at a rate of 0.50 L min^{-1} through an

136   impinger containing 5 mL of a DNPH solution in acetonitrile. The resulting solutions were analyzed by high-performance

137   liquid chromatography with a ultraviolet detector (HPLC/UV) (Smith et al., 1989). A 15-component hydrazone standard

138   (comprising formaldehyde-, acetaldehyde-, acrolein, acetone-, propionaldehyde-, crotonaldehyde-, methacrolein-,

139   butyraldehyde-, 2-butanone-, BnAld-, glyoxal-, valeraldehyde-, m-tolualdehyde-, methylglyoxal-, and hexaldehyde;

140   AccuStandard, Inc.) at a free carbonyl concentration of 30 μg mL^{-1} for each component was used for calibration. Separate

141   dihydrazone standards of glyoxal-DNPH and methylglyoxal-DNPH were also formulated. Carbonyls were separated

142   using a Hewlett-Packard (HP) 1100 HPLC system having an Agilent Zorbax ODS 4.6 x 250 mm, 5-µm column maintained

143   at 30°C eluted with binary acetonitrile-water gradient. A 10 µL injection volume was used for all standards and samples.

144   Carbonyls were quantified by UV absorption with a diode array detector set to 360 nm. Control and sample processing

145   were managed with HP ChemStation software. More highly oxidized gas-phase organic species were also collected with

146   a 60-cm, 4-channel XAD4-coated annular denuder for off-line analysis (Jaoui and Kamens, 2001). Once collected, the

147   denuders were extracted and analyzed according to the methodology described in section 2.4 below.

148

149 **2.3 Aerosol-phase: bulk parameter measurements**

150   Organic carbon (OC) was measured using a semi-continuous elemental carbon-organic carbon (EC-OC) instrument

151   (Sunset Laboratories, Tigard, OR) (Offenberg et al., 2007). The pumping system draws chamber effluent through a quartz

152   filter at a rate of 8 L min^{-1} with carbon-strip denuder to remove gas-phase organics that might interfere with the

153   measurement. With a sample collection time of 0.5 h and an analysis time of 0.25 h, the duty cycle for the measurement

154   of OC was 0.75 h (Lewandowski et al., 2015). The aerosol volume, size distribution, and total number density were

155   measured using a scanning mobility particle sizer (SMPS), (Model 3071A, TSI, Inc., Shoreview, MN) and a condensation

156   particle counter (CPC) (Model 3010, TSI, Inc., Shoreview, MN). The SMPS operating conditions were as follows: sample

157   flow 0.2 L min^{-1}; sheath flow 2 L min^{-1}; size scan from 19 to 982 nm.

158

159 **2.4 Molecular characterization of GP and PP oxygenated organic products**

160   A non-targeted chemical analysis was conducted focusing mainly on species bearing hydroxy and carboxylic groups

161   (Jaoui et al., 2004, 2013, 2018). For each experiment, six 47-mm glass fiber (GF) filters were taken for 24 h at a flow rate

162   of 16.7 L min^{-1}. A second set of samples used an in-line 60-cm XAD-4 coated annular denuder (followed by a GF filter)

163   and analyzed for gas-phase organic products (Jaoui and Kamens, 2001). After collection, GF filters were extracted by

164   sonication with 5 mL methanol for 1 h, and denuders were extracted with 30 mL 1:1 dichloromethane/methanol mixture

165   (Jaoui and Kamens, 2001). Prior to extraction, denuders and GF filters were spiked with *cis*-ketopinic acid (KPA), trans-

166   p-menth-6-ene-2,8-diol (PMD), and d$_{50}$-tetracosane (TCS) as internal/recovery standards (IS/RS). Denuder extraction

167   solvents were rotary evaporated to ~1 mL and filtered using 0.45-µm PTFE syringe filters. A 2 µL portion of this extract

168   was analyzed by GC-MS (Jaoui and Kamens, 2001). The remaining denuder and filter extracts were evaporated to dryness

169   under a gentle stream of N$_2$ at room temperature using an N-Evap evaporation bath (Organomation Associates, Inc.,

170   Berlin, MA), then derivatized with BSTFA (Jaoui et al., 2004). This technique provides a sensitive method for measuring

171   low levels of highly oxidized organic compounds, including semi- and intermediate-volatile compounds in the GP and

172   PP.

173   The GC-MS analysis was conducted on an Agilent GC (7890B) coupled with a quadrupole mass spectrometer

174   (5977B). The injector, heated to 270 ºC, was operated in splitless mode. Compounds were separated on a 60-m-long, 0.25-

175   mm-i.d. RTx-5MS column (Restek, Inc., Bellefonte, PA) with a 0.25-µm film thickness. The GC oven temperature was

176   initiated at 84 ºC, held for 1 min, then increased at 8 ºC min^{-1} to 200 ºC, followed by a 2-min hold, then an increase at 10

177   ºC min^{-1} to 300 ºC and a 15-min hold. The ion source, ion trap, and interface temperatures were 200, 200, and 300 ºC,

178   respectively. Mass spectra were collected in both the methane-chemical (CI) and electron ionization (EI) modes.

179

180   **2.5 Experimental and quality control procedures**

181   Before each experiment started, the chamber was flushed with zero air (hydrocarbon-free) for 24 h from an Aadco

182   clean generator (Cleves, OH, USA). Experiments were conducted in either the absence or presence of NOx. For

183   experiments with NOx, BnOH and NO were added to the chamber through flow controllers to the target concentration.

184   For experiments in the absence of NOx, the photolysis of H$_2$O$_2$ was the source of OH. H$_2$O$_2$ as a 50 % aqueous solution

185   was injected through a syringe pump into a heated glass bulb where it vaporized and then was mixed rapidly by the main

186   dilution air flow. For these experiments, BnOH was added as described above. Ammonium sulfate seed aerosol was also

187   introduced into the chamber for all experiments to serve as a condensing medium for semivolatile organic products that

188   might form. After the reactants reached steady state concentrations (24 hours), the background was characterized using

189   all instruments to check for artifacts including background GP and PP species. Background chamber air was also

190   characterized using off-line analysis of denuder and/or filters as described above. Previous studies show that BnAld and

191   to a lesser extent benzoic acid, benzyl benzoate and dibenzyl ether present either as impurity, or as decomposition products

192   upon BnOH exposure to air at room temperature or sonication (Urakami et al., 2000; Ferri et al., 2006; Abend et al., 2004).

193   Here we investigated the effect of chamber air, sonication, and BSTFA derivatization on BnOH artifacts as described in

194   the supplementary information (SI) in section 1. A small amount of BnAld impurity was detected using the direct injection

195   (DI) method and estimated to be <0.1% in the purchased solution. When BnOH was exposed to clean air in the chamber

196   in the absence of light, sonication, and/or BSTFA derivatization, our results show additional low level of BnOH

197   conversion to BnAld and benzoic acid using DI and BSTFA methods, which is similar to the findings of Abend et al.

198   (2004), Urakami et al. (2000), and Ferri et al. (2006). Additional results and descriptions are provided in section S1 (SI).

199   Experiments were initiated by turning on the lights and allowing the irradiated chamber effluent to reach SS

200   conditions over a 24-h period which permits active sampling by the on-line instruments and the collection of denuder and

201   filter samples for subsequent off-line analysis. For organic intermediates wall losses are typically not an issue due to

202   reactions being conducted within a Teflon chamber. This potential issue is mitigated further from operating the chamber

203   in a SS mode where compound loss and re-evaporation quickly comes to steady state. Short lifetimes of radical

204   intermediates with other gas-phase constituents also render a negligible wall-loss. The stability of BnOH in the chamber

205   was investigated and BnOH was found to be highly stable with results given in the SI (section S1). Denuders and GF filter

206   samples were also analyzed to probe reproducibility of the analytical technique. The analysis showed consistent results.

207   Gas and particle samples from BnOH photooxidation are dominated by oxygenated species, several not having

208   authentic standards, and thus a portion of each sample was derivatized. Initially, we eliminated peaks detected in blank

209   and background samples. For compounds having standards, comparisons were made between the retention times and mass

210   spectra (CI and/or EI mode) of the chamber-derived peaks and those of the standards. For compounds not having

211   standards, individual peak identifications were associated with a product peak only if its retention time and mass spectrum

212   was consistent with the fragmentation pattern of the BSTFA-derivatized compound. All recorded spectra in this study

213   were compared with those derived from reference standards, the literature, the NIST library, and an archive of mass

214   spectra from product compounds determined in our laboratory over the past twenty years.

215

3 Results and discussion

The initial conditions of the experiments conducted in this study are summarized in Table 1. Three NOx experiments were carried-out with initial BnOH ranging from 0.36 – 0.72 ppm and NO from 0.096 – 0.19 ppm. One experiment without NO$_X$ was conducted with initial H$_2$O$_2$ and BnOH levels of 3.0 and 0.32 ppm, respectively. NOx experiments were conducted at ~30% RH, and the H$_2$O$_2$ experiment at < 4% RH to minimize H$_2$O$_2$ uptake onto chamber surfaces. Chamber temperatures were set to 25 ℃. Each experiment was conducted for up to five days for samples requiring substantial masses or extended collection times and frequencies.

Steady state concentrations of NO, BnOH, O$_3$, and NOy for the four experiments are given in Table 2. The reacted BnOH and NO were calculated from the difference between the initial and steady-state concentrations. For NOx experiments, the range of reacted BnOH concentrations was 0.22 – 0.34 ppm having a reproducibility of 20–30%. Under these conditions, steady state concentrations of NOy, and O$_3$ were in the range of 0.08 – 0.16 and 0.011 – 0.15 ppm, respectively. With NO present at steady-state, peroxy-peroxy (RO$_2$–RO$_2$) reactions were minimized. A constant aerosol source was maintained for initial conditions given in Table 1. The major aerosol parameters measured (SOA, SOC, and OM/OC) are given in Table 3. SOC uncertainties were taken from the reproducibility of the semi-continuous measurement and typically better than 10% for a single run. For the organic mass (OM), the uncertainties are determined from the reproducibility of side-by-side filter measurements which are typically better than 5%. An estimate of the systematic errors due to minor changes in reactant concentrations, minor variations in chamber temperature, and similar factors bring the total uncertainty to between 15-25% for these parameters (Kleindienst et al., 2009). SOA/SOC values were then determined from the corrected data and given in Table 3. For experiments in the presence of NOx, SOA/SOC values ranged from 1.7-2.0. Similarly, in the absence of NOx, the measured SOA/SOC value was 2.1.

3.1 Secondary organic aerosol and secondary organic carbon yields

Secondary organic aerosol yield (Y$_{SOA}$) and secondary organic carbon yield (Y$_{SOC}$) were calculated from the following respective relationships Y$_{SOA}$ = SOA/ΔHC (1); Y$_{SOC}$ = SOC/ΔHC$_C$ (2) where SOA is the corrected organic aerosol mass concentration originated from filter measurements (6 filters) and ΔHC is the reacted BnOH concentration. SOC is the organic carbon concentration found in Table 3 and ΔHC$_C$ is the reacted BnOH carbon concentration. SOA and SOC were corrected for wall loss to the chamber which had previously been determined for organic aerosol to be 0.067 h^{-1} (Kleindienst et al. 2012). Uncertainties in the yield come from the experimental uncertainties in SOA and SOC

244   production and the reacted BnOH concentrations. The uncertainty in the reacted BnOH results from the reproducibility

245   of the initial and steady-state values and is estimated to range from 20 - 30% given the low volatility of BnOH and

246   challenges for introducing oxygenated species into the chamber in a consistent manner. Such challenges are also present

247   in a batch mode experiment given the difficulty to determine BnOH time profiles given its volatility and high reactivity

248   toward oxidants (Shilling et al., 2008; Kroll et al., 2007). Similar findings have been reported for sesquiterpenes oxidation

249   (Jaoui et al., 2013). As a result, aerosol yields of higher accuracy are often reported to be associated with steady state as

250   opposed to batch mode experiments (Shilling et al., 2008). Moreover, in this work we explored the possibility of BnOH

251   being taken up by ammonium sulfate (AS) seed aerosol prior to start of the irradiation or by SOA after it is initiated. This

252   test was conducted using GC-MS analysis of derivatized (BSTFA) and underivatized denuder and GF filter extracts

253   collected before and after the reaction starts (SI; Section S1). Under the experimental conditions used in this study, BnOH

254   was undetected in AS and SOA, thus limiting any participation in particle chemistry that may occur.

255   The production of aerosol, and thus the yield, were found to be highly sensitive to the precise initial conditions

256   (Tables 1, 3). Yields for the four experiments are shown in Table 3. Y_{SOA} values were determined for SOA concentrations

257   from 39.6 - 119.5 µg m^{-3} and ranged between 3.6 and 8.1%. Similarly, Y_{SOC} was measured for SOC concentrations from

258   23.2 – 58.9 µgC m^{-3} and found to range between 2.7 and 5.1%. In the absence of NO$_X$, SOA and SOC yields were 5.2

259   and 3.1 % measured for SOA and SOC concentrations of 52.9 µg m^{-3} and 24.8 µgC m^{-3}, respectively. For the two systems

260   at similar SOA concentrations ER890 and ER892, the SOA yield was higher for the experiment with NO$_X$. This may

261   result from the reaction of BnOH with NOx which tends to produce high levels of BnAld (Table 4), which may undergo

262   secondary reactions leading to additional SOA formation (see section 3.3). As expected, the data in Table 3 indicate that

263   Y_{SOA} and Y_{SOC} are lower at the lower SOA and SOC concentrations, respectively.

264   These SOA and SOC yields can be compared with other studies. Recently, Charan et al. (2020) reported SOA yields

265   for the photooxidation of BnOH in the presence of NO$_X$ with the initial OH coming from the photolysis of H$_2$O$_2$. Their

266   chamber was operated in a batch mode and SOA yields approaching unity were reported. By contrast, three additional

267   studies reported much lower SOA yields of 9%, 30%, and 41% from McDonald et al. (2018), Carter et al. (2005), and Li

268   et al. (2018), respectively. The yield reported by McDonald et al. (2018) was based on a multi-generation oxidation model;

269   that of Carter et al. (2005) was estimated as described in the original report, and that of Li et al. (2018) was based on

270   measurements in the presence of NOx and a surrogate urban hydrocarbon. The results of our study are much closer in

271   value to McDonald et al. (2018). The study by Charan et al. (2020) suggests that conditions can be found where BnOH

272   SOA yields are substantially greater than that found in this study and those previously reported. The major differences

273   between the Charan et al. study and the present work were the chamber-mode operation, the seed aerosol type and levels,

274   and the mix of oxidants used. While it can be difficult to compare the yields from the two studies some comments can be

275   made. (1) As noted, the Charan et al. yields result from conventional batch mode irradiations of BnOH, H_2O_2 and NO_X.

276   (2) SOA levels were measured using an SMPS which measures aerosol volume which is then converted to aerosol mass

277   using a density of 1.4 μg nL^{-1}. (3) Perhaps the biggest difference between the two studies is the use of an extremely high

278   initial seed aerosol mass, approximately two orders of magnitude higher than in this study. Thus, it is possible that an

279   adsorption mechanism played a part in contributing to the measured yields. (4) Finally, the use of high initial H_2O_2

280   concentrations relative to BnOH make it possible that H_2O_2 effectively competed with BnOH for OH via the reaction of

281   OH + H_2O_2 --> HO_2 + H_2O thus generating a system rich in HO_2. Thus, aging process may be more prominent than in our

282   study. The uncertainties associated with SOA and reacted BnOH measurements and wall loss correction are unlikely to

283   account for the differences in the two studies. However, SOA yields have been reported to increase considerably as a

284   function of initial seed aerosol (Zhang et al. 2014), as well as to increase with the OH radical exposure (Wang et al.,

285   2018). Qualitatively these two factors might bring the present SOA yields into reasonable agreement with Charan et al.

286   (2020), when data were extrapolated to similar seed aerosol and OH exposures. And as previously noted, in the low initial

287   seed aerosol used in our study no benzyl alcohol was detected in the seed aerosol or deposited on SOA. As further

288   plausibility for the results from the present study, Humes et al. (2022) recently reported yields from 12% - 18% for two

289   oxygenated aromatic species (1-phenoxy-2-propanol, and phenoxy-ethanol), compounds having similar structures to

290   BnOH.

291

292   **3.2 Reaction products identification**

293   Three methods were used in this study to identify oxygenated reaction products at the molecular level: (1) DNPH as

294   derivatizing agent for small carbonyls (Smith et al. 1989); (2) BSTFA as derivatizing agent for hydroxyl and carboxylic

295   compounds for GP and PP (Jaoui et al., 2004); and (3) direct injection (DI) method providing the capability for analysing

296   slightly polar to non-polar compounds without the use of derivatization (Jaoui and Kamens, 2001). For the BSTFA and

297   DI methods, the analysis of laboratory generated GP and PP products from BnOH oxidation shows a series of organic

298   compounds containing nitro, ketone, carboxylic acid, and/or alcoholic functional groups. Many of these compounds do

299   not have authentic standards and their identifications were based on the interpretation of the mass spectra of the derivatized

300 and/or underivatized compound (Jaoui and Kamens 2001; Jaoui et al., 2004, 2005). The identification should be regarded

301 as tentative except for compounds that have authentic standards. For the BSTFA method, the recognition of characteristic

302 ions was used to guide the analysis of mass spectra of the derivatives obtained in both electron ionization (EI) and chemical

303 ionization (CI) using methane as reagent gas. BSTFA reacts with -COOH and -OH groups to form BSTFA derivatives.

304 Characteristic ions are m/z 73, 75, 147, and 149. Adduct ions in CI from the derivatives include m/z $M^{+\cdot} + 73$, $M^{+\cdot} + 41$,

305 $M^{+\cdot} + 29$, and $M^{+\cdot} + 1$; fragment ions include m/z $M^{+\cdot} - 15$, $M^{+\cdot} - 73$, $M^{+\cdot} - 89$, $M^{+\cdot} - 117$, $M^{+\cdot} - 105$, $M^{+\cdot} - 133$, and/or

306 $M^{+\cdot} - 207$. The approach used for the identification is as follows: peaks detected in blank and background chamber samples

307 were eliminated first. A peak was associated with a reaction product only if its corresponding mass spectrum was

308 consistent with the fragmentation pattern of the BSTFA derivatization reagent. All recorded spectra were compared with

309 spectra derived from various reference compounds, authentic standard, NIST library, the PubChem website

310 (pubchem.ncbi.nlm.nih.gov), and/or by MS assignment. While the off-line technique is an integrated technique that

311 requires long sampling times, it does provide a sensitive method for products identification at the molecular level as well

312 as measuring low concentrations of highly oxidized organic compounds, and semivolatile compounds in the GP. Thus,

313 products found by this collection technique could be informative for possible precursors for the types of compounds that

314 may form in the PP. In the following discussion, data are first presented to support tentative identifications of oxidation

315 products in the GP and PP.

316 **Gas phase products.** GP measurements were made of major carbonyl products formed during the photooxidation of

317 BnOH including formaldehyde, acetaldehyde, acetone, methacrolein, 2-butanone, BnAld, glyoxal, and methylglyoxal.

318 Steady-state concentrations are given in Table 4. Under the conditions shown in Tables 1 and 2, high concentrations were

319 observed for BnAld and glyoxal, and to a lesser extent formaldehyde in experiments with NOx, and high concentrations

320 of formaldehyde, acetaldehyde, and to a lesser extent BnAld and glyoxal in the experiment without NOx. BnAld level

321 was a factor of ~5 higher in NOx experiments compared to H_2O_2 experiments, and formaldehyde a factor of ~36 lower.

322 Glyoxal and methylglyoxal concentrations largely were similar in both NOx and H_2O_2 experiments. The formation of

323 BnAld, glyoxal, and formaldehyde as major products (Table 4) have already been reported from the oxidation of BnOH

324 with yields of 25 ($\pm$ 5), 20 ($\pm$ 2), and 3.0% ($\pm$ 0.2), respectively (Bernard et al., 2013; Harrison and Wells, 2012).

325 GP samples were also collected on five-channel annular denuders. Each denuder sample was extracted and analyzed

326 directly with GC-MS without derivatization. The remaining extract was silylated, and GC-MS analyzed qualitatively.

327 Typical total ion chromatograms (TIC) of GP products detected and identified in this study are shown in Figure 1. Figure

328 1 shows portions of three TIC in +EI of GP samples taken from experiments ER889 at steady state (underivatized: Figure

329 1a), ER892 (underivatized: Figure 1b), and ER889 (silylated derivatives: Figure 1c). Peaks assigned in Figure 1 were

330 identified either by comparison with an authentic standard or by MS assignment. For clarity, only the main products are

331 shown, although several peaks could not be structurally identified. SOA generated from BnOH photooxidation is

332 dominated by oxygenated ring-opening products (see below). However, ring-retaining products were among the main

333 products observed in the GP including semivolatile organic compounds (SVOCs) (Figure 1c). Chromatograms associated

334 with the underivatized samples (Figure 1a, b) were used mainly to identify BnOH and BnAld in the system, although

335 several additional peaks absent in the background chromatogram were observed. At steady state, BnOH was not reacted

336 completely as it was detected in both systems only in the GP using both DI and BSTFA methods (Figure 1). BnAld was

337 detected in both systems in the gas and particle phases, although it was not present with BSTFA method because of the

338 absence of OH or COOH groups. Figure S3 shows EI mass spectra of BnAld identified using authentic standard, and

339 those associated with three peaks eluting at 11.3, 12.0, and 12.8 min. Although no structural information could be

340 associated with these three peaks, molecular weights of 152, 152, 138 Da (all derivatized and underivatized masses are

341 Dalton (Da) but are not designated as such hereafter), were tentatively obtained.

342 Select GP products containing OH groups identified in the present study are summarized in Table 5. Table 5 contains

343 proposed structures, molecular weights of the silylated derivatives (MW$_{BSTFA}$) and underivatized compounds (MW),

344 formula, and the 5 most intense ions associated with BSTFA derivatives in EI mode. Table 5 shows if GP products are

345 detected also in the PP. Figure S4 shows EI mass spectra associated with selected peaks observed in Figure 1c, including

346 BnOH-1TMS, benzoic acid-1TMS, catechol-2TMS, and 2-hydroxybenzyl alcohol-2TMS. 2-Hydroxybenzyl alcohol-

347 2TMS (2OHBnOH) peak eluted at 21.4 min was one of the largest peaks detected in the chromatogram in Figure 3c. The

348 2OHBnOH-2TMS EI mass spectrum (Figure S4, bottom) shows strong characteristic fragments ions at m/z 73, 179 (M$^{+\cdot}$

349 - 89), 253 (M$^{+\cdot}$ - 15), 268 (M$^{+\cdot}$), and its corresponding CI mass spectrum shows ions at m/z 253 (M$^{+\cdot}$ - 15), 179 (M$^{+\cdot}$ - 89)

350 and weak adducts at M$^{+\cdot}$ + 1, M$^{+\cdot}$ + 29, and M$^{+\cdot}$ + 41 that are consistent with the presence of two (-OH) groups, indicating

351 a BSTFA derivatized molecular weight of 268 Da. Bernard et al (2013) have identified 2OHBnOH and catechol in the

352 GP of the reaction of BnOH and OH radicals. In our study, catechol was observed only in the H$_2$O$_2$ system in the PP.

353 Additional peaks were observed, which their mass spectra are consistent with products bearing OH and/or COOH groups,

354 however, their structural identification could not be obtained due to lack of authentic standards and the complexity of the

355   interpretation of their mass spectra. BnAld was reported to undergo secondary reactions (Sankar et al., 2014) and may

356   play an important role as precursor for some oxygenated species observed in this study.

357   **Particle phase products.** One of the advantages of conducting experiments in SS mode is collecting sufficient gas and

358   aerosol masses on denuders and filters for qualitative and quantitative offline analysis. In this study, aerosol collected on

359   GF filters were solvent extracted, with the resulting extracts subjected to BSTFA derivatization followed by GC-MS

360   analysis. SOA generated from both NOx and H_2O_2 systems was dominated by oxygenated organic compounds, for which

361   mass spectra for more than 50 species have been recorded. These species may have undergone several generations of

362   atmospheric oxidation. Several individual large peaks have been detected in addition to a significant number of small

363   peaks as shown in Figure 2. Figure 2 shows portions between 9 and 28 min of the TIC chromatograms of the silylated

364   derivatives of the aerosol extracts associated with BnOH/NOx (top) and BnOH/H_2O_2 (bottom). The portion after 28 min

365   is discussed in the next section. The chromatograms in Figure 2 can be directly compared because the chamber air sampled

366   and the amount of extract analyzed for each system were the same. This evaluation revealed that more than 70% of peaks

367   eluted from each system are identical, suggesting similar chemistry is involved in BnOH reaction products formed in the

368   presence and absence of NOx. In addition, a series of peaks dominated by fragments with odd *m/z* were observed only in

369   BnOH/NOx and their mass spectra were associated with nitrogen containing compounds as discussed in the NACs section

370   below. This suggests that the composition of a portion of SOA produced in the presence of NOx is different than that

371   formed in the absence of NOx, which can be clearly illustrated by the filters and extracts color shown in Figure 2 (bottom).

372   Consistent with the presence of nitroaromatics, filter F2 and methanol extract (E2) has lost most of the color seen in F1

373   and E1. The presence of NOx in the system produced material (filter F1) of a deep brown color. Most species structurally

374   identified in this study have not been reported in the literature, and mass spectra associated with several peaks are provided

375   either in the main manuscript or in the SI. Additional reaction products (e.g., oligomers, organonitrates) might have been

376   present in the SOA but could not be detected based on the analytical techniques used in this study. Note that formulae, in

377   particular chemical structure, could not be obtained for several peaks recorded in this study due to challenges interpreting

378   their mass spectra. A set of compounds identified and detected before 28 min in the present study are summarized in

379   Table 5.

380   Ring retaining products (e.g., 2-hydroxy benzyl alcohol, benzoic acid, 4-hydroxy benzoic acid, and catechol) were

381   detected in the PP in both systems. As noted above, some ring-retaining products were detected also in the GP as shown

382 in Table 5. Salicylaldehyde and 3-hydroxybenzaldehyde were present only in the GP. These two hydroxy-aldehydes may

383 undergo additional secondary reactions leading to some ring-opening products observed in this study. Representative EI

384 mass spectra of the TMS-derivatives associated with four compounds are shown in figure 3 including benzoic acid,

385 benzene-1,2-diol (catechol), 4-hydroxybenzoic acid, and 2-hydroxybenzyl alcohol. Additional EI and CI mass spectra are

386 shown in figures S4 and S5 in the SI. The EI mass spectrum of the BSTFA derivative of 2-hydroxybenzyl alcohol

387 displayed in figure 3 shows abundant fragment ions at m/z 73, 147, 267 (M$^{+\cdot}$), 253 (M$^{+\cdot}$ − 15), and 179 (M$^{+\cdot}$ − 89), and

388 weak ions at m/z 91, 223 and 163. The corresponding CI mass spectrum displayed in figure S4d shows abundant fragment

389 ions at m/z 268 (M$^{+\cdot}$), 253 (M$^{+\cdot}$ − 15), and 179 (M$^{+\cdot}$ − 89) and adduct ions at m/z 293 (M$^{+\cdot}$ + 29) and 309 (M$^{+\cdot}$ + 41). This

390 fragmentation pattern is consistent with the presence of a compound with two hydroxyl groups and a benzene ring (m/z

391 91) having molecular weight 268 for the BSTFA derivative, and MW 124 for its underivatized form. Similarly, the BSTFA

392 EI mass spectrum of 4-hydroxybenzoic acid (Figure 3c) shows characteristic fragment ions at m/z 73, 193 (M$^{+\cdot}$ - 89), 223

393 (M$^{+\cdot}$ - 60), 267 (M$^{+\cdot}$ - 15) and 282 (M$^{+\cdot}$), and its CI mass spectrum fragment ions at m/z 73, 193, 67 and adducts at 283,

394 and 311. Again, these fragments and adducts are consistent with the presence of two (-OH) groups and a molecular weight

395 of the derivatized compound of 282 and 138 for the underivatized compound. The presence of a peak at m/z 153 (M$^{+\cdot}$ -

396 117) is consistent with a compound bearing an organic acid group. The EI mass spectra recorded in this study for 2-

397 hydroxybenzyl alcohol and 4-hydroxybenzoic acid are identical to the reference NIST spectrum (webook.nist.gov). Figure

398 S5 shows EI mass spectra associated with four peaks eluted at 12.86, 15.58, 16.24, and 19.78 min consistent with the

399 fragmentation pattern of BSTFA derivatives, although their structures could not be obtained.

400 **Highly oxygenated compounds (HOCs).** Recent studies show that highly oxygenated compounds (e.g., HOMs) play an

401 important role in understanding SOA formation (Berndt et al. 2016, Jaoui et al., 2019; 2021 and references therein, Piletic

402 and Kleindienst, 2022). These compounds may result from several generations of atmospheric oxidation. In this study,

403 several ring-opening products eluted late in the chromatograms (RT > 25 min), with a relatively high O:C ratio of > 1.3

404 likely contributes to their condensation in the PP, were detected. Three groups of these oxidation products were detected

405 in the PP in both systems. Figure 4 shows the portion between 25 and 34 min of selected GC-MS extracted-ion

406 chromatograms where these groups (color coded) elute and uses the selected ions m/z 423, 437, and 525 (merged in one

407 chromatogram) to best illustrate them: (a) BnOH/NOx; (b) BnOH/H$_2$O$_2$; (c) chamber background. Groups 1, 2, and 3

408 consist of three (green), eight (blue) and four (red) peaks, respectively, and are completely absent from the background

409 chromatogram (figure 4c). Results from a comprehensive interpretation of EI and CI mass spectra associated with peaks

410 shown in figure 4 enabled the identification of several isomers associated with each group. Figure 5 displays three EI

411 mass spectra associated with each group main peak, along with proposed structure and chemical formulae. Table 6 gives

412 the major highly oxygenated compounds identified in this research, including the main peaks from each of these groups,

413 in the order of their underivatized molecular weight. Table 6 gives the chemical formulas, O:C mass ratio, the five most

414 abundant ions associated with each TMS derivative in methane-CI and EI modes, the molecular weights of the

415 underivatized (MW) and TMS-derivatized compounds (MW$_{BSTFA}$), and the proposed chemical structures of the

416 compounds.

417   Group 1 consists of *meso*-tartaric acid (*m*TA) (Rt 26.04 min), and *L*-/*D*-tartaric acids (*l*TA/*d*TA) (Rt 27.66 min)

418 identified based on authentic standards. The mass spectra of BSTFA derivatives of *l*TA and *d*TA standards (Figure S6,

419 SI) are very similar (eluting at the same time) and are only slightly different from the *m*TA (Figure S6: SI); however,

420 *l*TA/*d*TA and *m*TA elute at two different retention times (Figure 4, S6). The peak associated with *m*TA, and *l*TA/*d*TA are

421 among the largest peak observed in this portion of the chromatograms. Note, *l*TA isomer is the most abundant tartaric

422 acid present in nature (DeBolt et al., 2006). The fragments and adducts observed for the peak eluting at 25.19 min are

423 similar to those of mTA and d-/lTA and are consistent with the presence of four OH groups, a MW of 452 for the

424 derivatized compound and 164 for the underivatized compound, and a $C_4H_6O_6$ chemical formula. Tartaric acid has been

425 reported in ambient aerosol (Rohrl and Lammel, 2002; Gowda et al., 2016) and in chamber 1,3-butadiene SOA (Jaoui et

426 al., 2014). Recent studies suggest that tartaric acid and other hydroxy carboxylic acids undergo heterogeneous OH reaction

427 in aqueous solution, with the presence and position of OH group(s) playing an important role in fragmentation and

428 functionalization of organic aerosol (Cheng et al., 2016).

429   Group 2 consists of eight peaks (figure 4: blue) eluting between 28.5 and 31.5 min. The EI and CI mass spectra

430 associated with each peak display similar fragment and adduct ions across the range of 50 to 600 Da. The interpretation

431 of these mass spectra allows us to infer the molecular weight (MW) of the underivatized compounds as 164 and MW$_{BSTFA}$

432 of 452 for the TMS derivatives. The BSTFA CI mass spectrum of the peak eluted at 29.48 (largest peak) shows

433 characteristic fragment ions at m/z 73, 437 [M$^{+\cdot}$ -15], 363 [M$^{+\cdot}$ - 89], and 305 [M$^{+\cdot}$ - 105], and an adduct at 453 [M$^{+\cdot}$ + 1],

434 481 [M$^{+\cdot}$ + 29], and 493 [M$^{+\cdot}$ + 41]. These fragments and adducts are consistent with the presence of four OH groups and

435 an MW of 452 for the derivatized compound and 164 for the underivatized compound. The presence of peaks at m/z 347

436 [M$^{+\cdot}$ - 105], and 335 (M$^{+\cdot}$ – 117) are consistent with a compound bearing alcoholic and carboxylic OH groups

437 simultaneously. This mass spectrum is similar to the one from methyltartaric acid reported previously from isoprene

438   oxidation by our group (Jaoui et al., 2019). The silylated methyltartaric acid mass spectrum (Jaoui et al., 2019) and mass

439   spectra associated with group 2 are only slightly different, however, they elute at different retention times. The peaks have

440   been tentatively identified as isomers of trihydroxy-oxo-pentanoic acid, with the structure of 4-oxo-D-arabonic acid

441   isomer shown in Table 6.

442   Group 3 consists of four peaks eluting between 32.5 and 34 min (figure 4: red). The EI and CI mass spectra associated

443   with each peak display similar fragment and adduct ions across the range of 50 to 600 Da. As a descriptive example, an

444   EI mass spectrum is shown in Figure 5 for peak eluted at 33.1 min. A comprehensive interpretation of EI and CI mass

445   spectra associated with group 3 peaks (Figures 4, 5), allows us to infer the molecular weight (MW) of the underivatized

446   compounds as 180, and MW_{BSTFA} of 540 for the TMS derivatives, with a chemical formulae $C_5H_8O_7$. The compounds

447   corresponding to these four peaks were identified as isomers of C_5-trihydroxydicarboxylic acids. This identification is

448   tentative due to the absence of authentic standards, except for peak eluting at 33.47, which was identified as pentaric acid

449   (Table 6) based on authentic standard. The spectra of BSTFA derivatives of the remaining three red peaks are only slightly

450   different from the pentaric acid spectrum (Figure 6); however, they elute at different retention times. The EI mass spectra

451   are also similar to those reported in the literature for a set of C5-aldaric acids-TMS derivatives including xylaric, arabinaric

452   and ribaric acids (Hinton et al., 2008; https://pubchem.ncbi.nlm.nih.gov). Figure 6 shows the structure of pentaric acid

453   and its four isomers (a), the spectra associated with BSTFA derivative of pentaric acid observed in BnOH SOA (b: EI

454   mode), (c: CI-CH$_4$ mode), and standard (d: EI mode). Figure 6 also shows the structure of the main fragments observed

455   in BSTFA derivative of pentaric acid in EI mode including m/z at 540, 525, 407, 292, 147, and 73 Da. Pentaric acid and

456   its isomers (aldaric acids) are reported to be formed from the oxidation of aldopentose (Hinton, 2008; Derrien et al., 2018),

457   but no evidence has been provided for its presence in SOA samples. In the present study, we successfully identified aldaric

458   acids from the oxidation of BnOH in SOA samples.

459

460   **Nitroaromatic compounds (NACs).** NACs of secondary origin are a possible contributor to urban OA and not only

461   adversely affect human health and the environment but impact the aerosol optical properties and the atmospheric radiation

462   balance. By understanding the sources of NACs in ambient particles and their chemical identities, we can evaluate their

463   impact on the climate, environment, and human health. Recently, the analytical capabilities associated with BSTFA

464   derivatization have been extended to NACs bearing hydroxyl and carboxylic acid groups (Jaoui et al., 2018). Mass spectra

465   of most silylated NACs, especially methane-CI, are highly specific, reproducible, and produce characteristic fragments

466 useful in determining structural information and molecular weight, when authentic standards are not available (Jaoui et

467 al., 2018). In this study, a detailed analysis of mass spectra associated with peaks in chromatograms Figure 1c (GP) and

468 Figure 2 top (PP) reveals the presence of several peaks presenting similar fragmentation patterns as those reported by

469 Jaoui et al. (2018) for species bearing hydroxyl, carboxylic, nitro groups, and benzene ring. Figure 7 shows the portion

470 between 23 and 42 min of two +EI extracted ion chromatograms for the BSTFA derivatives at m/z 210, 165 (IS), 299 (IS),

471 300, 298, 372, 388 (merged in one chromatogram) associated with BnOH/NOx (top) and BnOH/H_2O_2 (bottom). The EI

472 and/or CI mass spectra of selected nitroaromatic standards can be found in Jaoui et al. (2018), and additional representative

473 subset of the derivatives are displayed in Figures S7 (SI). For clarity, figure 7 inset shows an expanded portion of the top

474 chromatogram between 26.7 – 28 min. Table 7 contains proposed identification of NACs detected in this study, along

475 with molecular weights, formulae, main 5 intense ions associated with CI and EI mass spectra of the derivatives, proposed

476 structure, and the GP to PP peak area ratio.

477   NACs with the highest confidence assignment are those identified by comparing their retention times, EI, and CI

478 mass spectra with those of reference standards, and NACs with low levels of confidence are those (1) that have been

479 identified previously in ambient PM or in smog chamber studies, (2) their EI mass spectra exist in the literature, or (3)

480 their molecular weights and numbers of OH, COOH, and NO_2 groups are simply consistent with the CI and EI mass

481 spectrum (Jaoui et al., 2018). A total of fourteen peaks associated with NACs were detected in this study. 3-Nitrobenzyl

482 alcohol, 4-nitrocatechol, 2-hydroxy-5-nitro benzyl alcohol, and 2-nitrophloroglucinol were identified based on authentic

483 standards. Three peaks eluted at 33.76, 34.70, and 34.76 having similar mass spectra as 2-nitrophloroglucinol (main peak)

484 eluted at 35.62 min were detected. They were tentatively associated with homologous series of 2-nitrophloroglucinol

485 including 3-nitrobenzene-1,2,4-triol, 5-nitropyrogallol, and 4-nitro-1,2,3-benzenetriol (not shown in Table 7). Similarly,

486 three additional peaks having similar mass spectra as 2-hydroxy-5-nitrobenzyl alcohol were observed and were tentatively

487 associated with homologous series of 2-hydroxy-5-nitrobenzyl alcohol including 4-hydroxy-2-nitrobenzyl alcohol. The

488 EIC in figure 7 (top) includes a series of four peaks observed only in the PP eluting at 35.94, 36.60, 38.18 min, whose

489 mass spectra were consistent with the presence of molecular weight 185 and 401 for the underivatized and derivatized

490 compounds, respectively. Based on similarity of their mass spectra, they were tentatively identified as structural

491 homologue of 3,4-dihydroxy-5-nitrobenzyl alcohol (Table 7) with $C_7H_7NO_5$ formulae. As can be seen in figure 7 (bottom),

492 NACs peaks were not detected in BnOH/H_2O_2 SOA extract, consistent with the formation of NACs in the presence of

493 NOx. All NACs were detected in both GPs and PP (Table 7), except 2-nitrophloroglucinol and 3,4-dihydroxy-5-

494 nitrobenzyl alcohol and their isomers were observed only in the PP consistent with their low volatility. This result suggests

495 that NACs may be formed in the GP, and partition to the PP for those with low volatility, although PP reactions may

496 occur as suggested by Charan et al. (2020) who analyzed only PP. 4-Nitrocatechol and 2-nitrophloroglucinol were among

497 the largest NAC peaks observed in our study (Figure 7). All three experiments conducted in this study were analyzed for

498 NACs to probe reproducibility of the BSTFA method and showed consistent results. 2-Nitrophloroglycinol, 4-

499 nitrocatechol and other NACs has been reported in PM collected in Pico Mountain Observatory, Pico Island in the Azores

500 archipelago by Ikemori et al., (2019). A series of NACs have been reported recently by Charan et al. (2020) in BnOH

501 SOA using off-line UPLC/ESIQ-ToFMS (ultra-high-performance liquid chromatography electrospray ionization

502 quadruple time of flight mass spectrometry), and the structure assigned to formulas obtained from MassLynk software

503 was based on expected oxidation products and MS/MS analysis. These observations support the identification of NACs

504 reported in this study. 4-Nitrophenol was reported in the GP by Bernard et al., (2013) at low yield and by Charan et al.

505 2020 in SOA from the OH radical oxidation of BnOH but was not detected either in the GP or the PP in this study.

506

507 **3.3. Mechanism of product formation**

508 Based on known GP reactions for aromatic compounds, a schematic representation for the reaction of BnOH with

509 OH is presented in schemes 1-3. It is developed to understand the chemistry leading to the main GP and PP products

510 identified experimentally in this study including HOCs and NACs. These schemes incorporate the latest experimental,

511 quantum and kinetic developments of the fate of peroxy/alkoxy benzoyl radicals including autooxidation (Wang, 2015;

512 Sankar et al. 2014, and Namysl et al. 2020). The lines shown in these schemes are either one step or multistep pathways.

513 Rate constants at room temperature of BnOH with OH radical, O_3, and NO_3 radical of 2.8 10^{-11}, 6 x 10^{-19} (upper limit),

514 and 4.0 x 10^{-15} cm^3 $molecule^{-1}$ s^{-1}, respectively, have been reported in the literature (Harrison and Wells, 2009, 2012;

515 Bernard et al., 2013). This suggests that the day-time oxidation of BnOH will be mainly initiated by OH radicals. The

516 reaction for O_3 and NO_3 radical are not included in schemes 1-3, although they are expected to be formed as minor

517 products in our systems.

518 The reaction of BnOH with OH radicals is initiated primarily by H atom abstraction from the external CH_2 group

519 leading to BnAld, and OH addition to the aromatic *ipso* (C1) and *ortho* (C2 or C6) positions to form two alkyldihydroxy

520 adducts R1 and R2 (scheme 1). The OH addition to the *para* (C3, C5) and *meta* (C4) position was reported to be not

521 favourable based on theoretical study of Wang, (2015). Scheme 1 shows mechanistic pathways leading to the formation
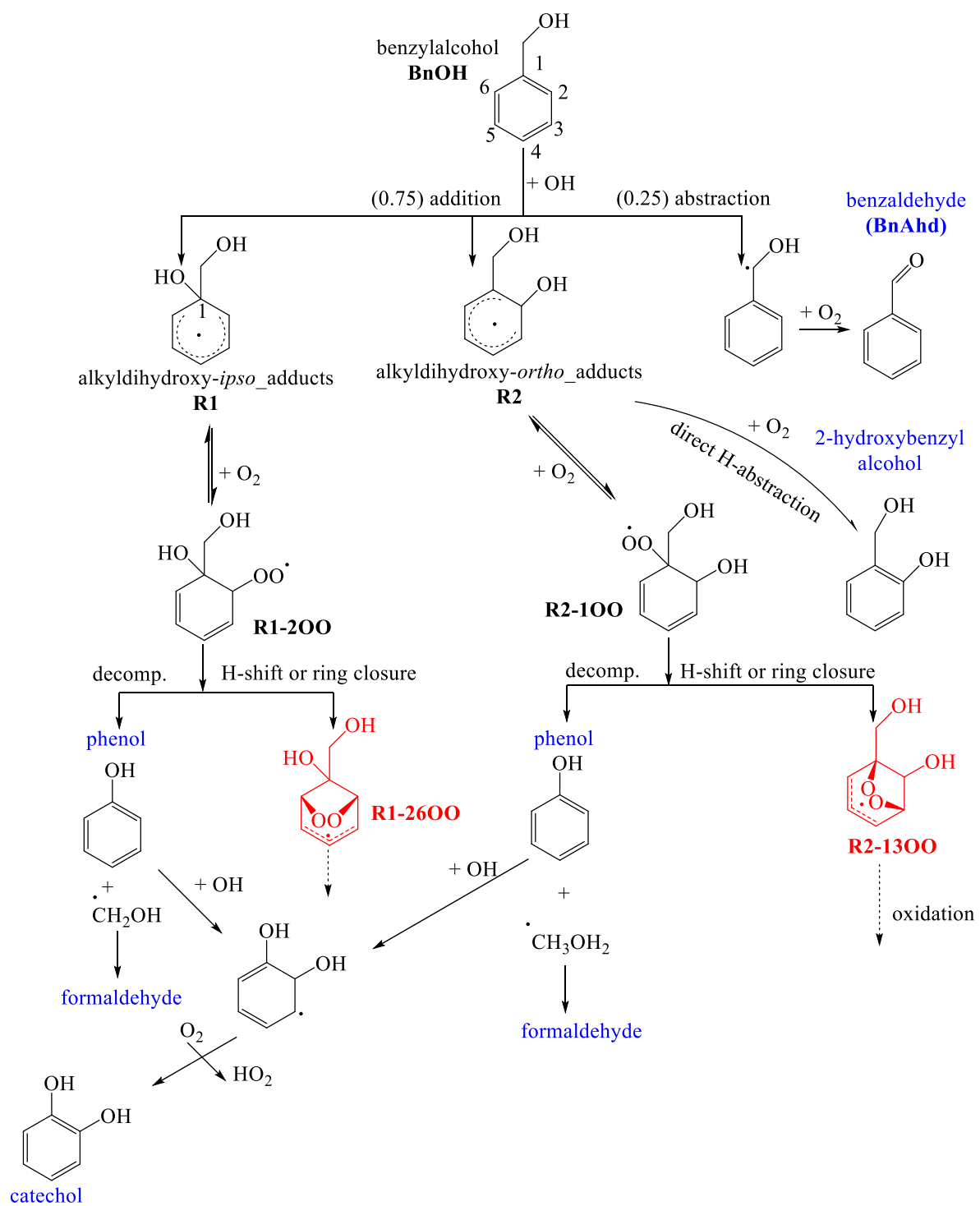
Scheme 1. Initial reaction pathways proposed to produce selected products detected in this study (blue color) in the gas or PP (Table 5). R1-26OO and R2-13OO intermediates undergo further reactions leading to ring-opening products as shown in scheme 3.

527   of stable products (blue) including BnAld, 4-hydroxybenzyl alcohol, 2-hydroxybenzyl alcohol, phenol, formaldehyde,

528   and catechol. The initial branching ratios shown in scheme 1 are those reported by Wang (2015), obtained by combining

529   quantum chemistry calculations and experimental work from the literature. BnAld was observed in this study in the

530   presence and absence of NOx, and its secondary chemistry may lead in part to oxygenated compounds observed in this

531   study (Bernard et al., 2013). Due to large number of possible intermediates formed (Wang, 2015), only selected pathways

532   energetically favourable leading to some products observed in this study are considered. We refer the readers to Wang

533   (2015) paper for an in-depth theoretical analysis of mechanistic pathways leading to the formation of selected reaction

534   products. The adduct R1 reacts rapidly through addition of O_2 to the ortho (C2) to produce peroxy radicals R1-2OO, The

535   O_2 addition to para position (C4) leading to R1-4OO peroxy radicals (not shown in Scheme 1) was found to be

536   endothermic, therefore negligible (Wang, 2015). Radicals R1-2OO undergo intramolecular H-shifts or ring closures to

537   form a stable bicyclic intermediate R1-26OO (red). Similarly, R2 reacts rapidly with O_2 to form peroxy radical R2-1OO

538   intermediate, which itself undergoes intramolecular H-shifts or ring closures to form a stable bicyclic intermediate R2-

539   13OO (red). R1-26OO and R2-13OO intermediates undergo further reactions leading to ring-opening products as shown

540   in scheme 3 below. 2-Hydroxybenzyl alcohol was proposed by Wang (2015) to form through the reaction of R2 with O_2

541   involving rapid direct H-abstraction. A possible formation pathway of phenol is decomposition of the peroxy radicals R1-

542   2OO and R2-1OO through CH_2OH radical elimination (Bernard et al., 2013). CH_2OH radical reacts rapidly with O_2 to

543   produce formaldehyde. Catechol was proposed to originate from the reaction of OH radicals with phenol (Atkinson et al.,

544   1992) and with 2-hydroxybenzyl alcohol (Bernard et al., 20013).

545   NACs observed in this study (Table 7) are expected to be formed through reaction of OH radicals with BnOH in the

546   presence of NO_2. Scheme 2 briefly summarizes the main mechanistic pathways leading to BnOH NACs, which follow

547   similar chemistry as those reported for toluene, benzene, and xylenes (Jenkin et al., 2003; Vidovic et al., 2018) and

548   summarized by Wang et al., (2019). The steps shown in scheme 2 are multi-steps and the reader should consult the

549   reference papers above for more in depth information. NACs are proposed to originate from secondary reactions of

550   catechol, 1,3,5-trihydroxy benzene, and 4-hydroxybenzyl alcohol with OH radicals in the presence of NO_2 (scheme 2).

551   These intermediates are proposed to be originated from R1, R2, and R3 adducts. Additional pathways could be initiated

552   via less well understood aqueous-phase nitration (Kroflic et al., 2018). 4-Nitrocatechol is proposed to be initiated through

553   the reaction of catechol with OH radicals in the presence of NOx (Finewax et al., 2018). 4-Hydroxy-2-nitrobenzyl alcohol

554   is proposed to be likely originated from the alkyldihydroxy-para-adduct formed from the OH addition to para position

555 (scheme 2). 2-Nitrophloroglucinol and 3,4-dihydroxy-5-nitrobenzyl alcohol follow similar reactions involving R3 adduct,

556 OH radicals, and NO_2. According to Wang (2015) calculation, at high NO_2 (100 ppbv) the reaction of R1 with NO_2 can

557 compete to a minor degree with the reaction with O_2, therefore R1 possibly forms minor amounts of nitrobenzyl alcohol.
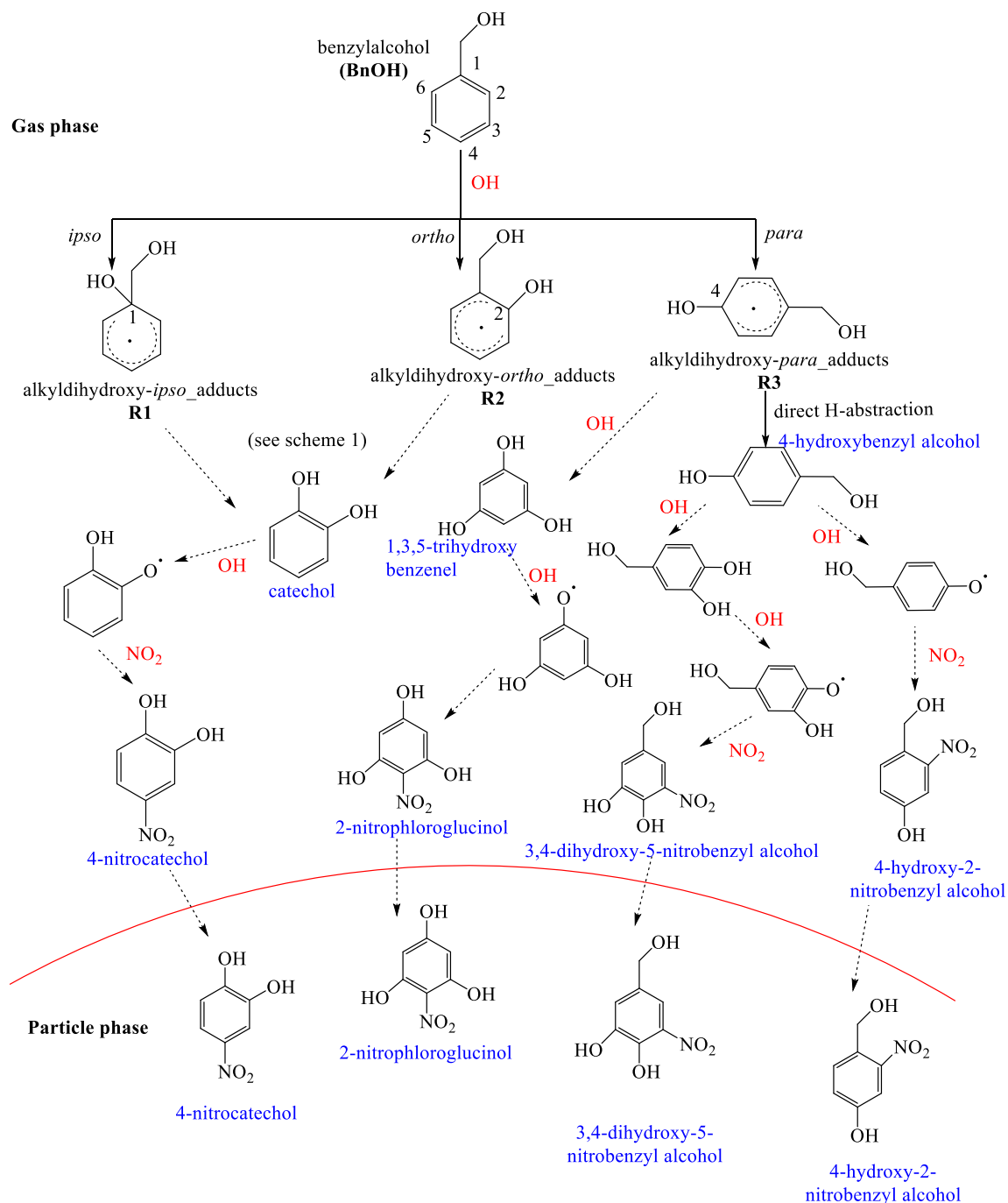
558

559

560 **Scheme 2.** Proposed mechanism for selected NAC species observed in this study.

561   HOCs were detected in the PP from the oxidation of BnOH in both low and high NOx systems (Table 6). Mechanistic

562   pathways based on theoretical studies leading to several HOCs (e. g. HOMs) from the atmospheric oxidation of biogenic

563   and aromatic hydrocarbons have been reported recently in the literature involving unimolecular reaction through

564   autoxidation, and peroxy and/or alkoxy radical isomerization (Wang, 2015; Jaoui et al., 2021; Piletic and Kleindienst,

565   2022). The formation of selected HOCs observed in this study is consistent with the following pathways proposed in

566   scheme 3 involving R2-13OO radical as the starting material. R1-26OO adduct undergoes similar reactions leading to

567   butenedial and 2,3-epoxy-butanedial as shown in scheme S1 (SI). Tartaric acid, 2,3,5-trihydroxy-4-oxo-pentanoic acid,

568   and pentaric acid, observed in this study for the first time, are proposed to be initiated by the oxidation of butenedial/2,3-

569   epoxy-butanedial, 5-hydroxy-4-oxo-2-penatenal, and 4-hydroxy-2,3-epoxypentandial (scheme 3). The mechanism
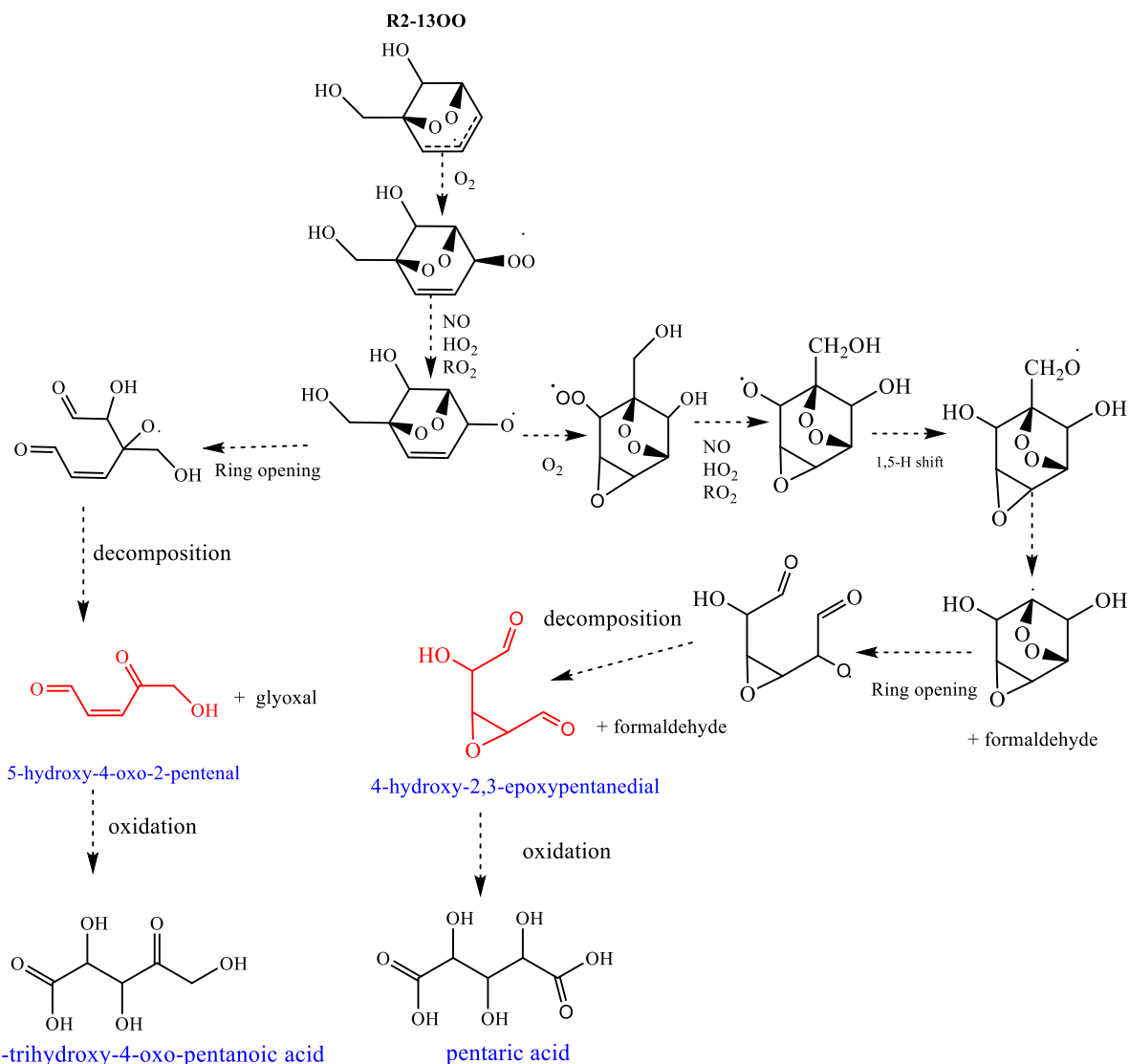
570

571   **Scheme 3.** Proposed mechanism for selected highly oxygenated compounds observed in this study.

572

573   leading to butenedial/2,3-epoxybutanal, 5-hydroxy-4-oxo-2-penatanal (scheme S1) was reported by Wang (2015) from

574   the OH oxidation of BnOH, therefore is not shown in scheme 3. Tartaric acid present in the PP at high level (Figure 4), is

575   proposed to be formed through the oxidation of butenedial and/or 2,3-epoxybutanal through classical oxidation of

576   aldehydes and alkenes to carboxylic acid (not shown in scheme 3). Similarly, 2,3,5-trihydroxy-4-oxo-pentanoic acid and

577   pentaric acid are proposed to rise from the oxidation of 5-hydroxy-4-oxo-2-pentenal, and 4-hydroxy-2,3-

578   epoxypentanedial, respectively following similar mechanistic pathways reported by Jaoui et al. (2021) for the formation

579   of methyltartaric acid from 4-hydroxy-2-methyl-but-2-enal involving peroxy and alkoxy radical isomerization (not

580   reported here). In this study, a new mechanism is proposed in scheme 3 leading to the formation of 4-hydroxy-2,3-

581   epoxypentanedial, which is the starting material for pentaric acid formation. It involves several intermediate steps

582   including unimolecular H migration (e.g., 1,5-H shift), ring opening and decomposition. Formaldehyde and glyoxal

583   observed in this study are also shown in scheme 3.

584

585   **4. Summary**

586   In the present manuscript, laboratory experiments were conducted to investigate SOA formation from the oxidation

587   of benzyl alcohol in the presence and absence of NO$_x$. Chamber aerosol collected under these conditions has been

588   analyzed for organic mass to organic carbon ratio, and aerosol yield. In addition, the chemical composition of the gas

589   phase and SOA was analyzed using derivative-based methods followed by gas chromatography-mass spectrometry and

590   high-performance liquid chromatography analysis of the derivative compounds. More than 50 oxygenated organic

591   compounds in the gas and particle phases were identified. While a detailed non-targeted analysis has been made, our

592   primary focus has been to examine highly oxygenated and nitroaromatic compounds. The major components include ring-

593   opening products with high oxygen to carbon ratio (e. g. malic acid, tartaric acid, arabic acid, 2,3,5-trihydroxy-4-oxo-

594   pentanoic acid, and pentaric acid) and ring-retaining products (e. g. benzaldehyde, benzoic acid, catechol, 3-nitrobenzyl

595   alcohol, 4-nitrocatechol, 2-hydroxy-5-nitrobenzyl alcohol, 2-nitrophloroglucidol, 5-(hydroxymethyl)- 3-nitro-1,2-benzyl

596   diol). The presence of some of these products in the gas and particle phases simultaneously provides evidence of their

597   gas/particle partitioning. These oxygenated oxidation products made dominant contributions to the SOA particle

598   composition in both low and high NOx systems. Yields, organic mass to organic carbon ratio, and proposed reaction

599   schemes for selected compounds are provided.

600 Finally, a set of reaction pathways are proposed that accounts for selected reaction products observed in this study

601 from BnOH photooxidation in the presence of OH radicals, including NACs and HOCs. The proposed mechanism is

602 based on (1) theoretical studies reported previously in the literature and (2) mechanisms associated with aromatics

603 oxidation (e.g., benzene, toluene, xylenes…). New pathways were proposed for the formation of newly observed highly

604 oxygenated compounds tartaric acid, 2,3,5-trihydroxy-4-oxopentanoic acid, and pentaric acid. Butenedial/2,3epoxy-

605 butandial, 5-hydroxy-4-oxo-2-pentenal, and 4-hydroxy-2,3-expoxypentanedial were proposed as the starting intermediate

606 species leading to these highly oxygenated compounds. While theoretical studies involving unimolecular reactions were

607 developed focusing mainly on ring-containing products (Wang, 2015, Piletic and Kleindienst, 2022), similar theoretical

608 investigations focusing on linear species (Jaoui et al., 2021) as HOCs reported in this study will help strengthen the

609 pathways proposed here.

610 The results of this study potentially have atmospheric implications for areas impacted by benzyl alcohol including

611 urban and indoor areas and contribute to understanding the formation of ambient SOA from oxygenated anthropogenic

612 precursors. Nitroaromatics are pollutants of concern due to their toxicity, light-absorption properties, and relatively long

613 residence times in the environment. HOCs may partition into pre-existing particles or be involved in new particle

614 formation.

615
616
617

618 *Data Availability.* The data used in this study can be found at: https://catalog.data. gov/dataset/epa-sciencehub. DOI:
619 10.23719/1527893.

620

621 *Competing interests.* The authors declare no competing financial interest.

622

627

628

629

630 **References**

631 Abend, A. M., Chung, L., Bibart, R. T., Brooks, M., and McCollum, D. G.: Concerning the stability of benzyl alcohol:

632 formation of benzaldehyde dibenzyl acetal under aerobic conditions, J. Pharm. Biomed. Anal., 34, 5, 957-962,

633 doi:10.1016/j.jpba.2003.11.007, 2004.

634

635 Akherati, A., Cappa, C. D., Kleeman, M. J., Docherty, K. S., Jimenez, J. L., Griffith, S. M., Dusanter, S., Stevens, P. S.,

636 and Jathar, S. H.: Simulating secondary organic aerosol in a regional air quality model using the statistical oxidation

637 model - Part 3: Assessing the influence of semi-volatile and intermediate-volatility organic compounds and NOx, Atmos.

638 Chem. Phys., 19, 4561–4594, 2019.

639

640 Alton, M. W., and Browne, L. C.: Atmospheric chemistry of volatile methyl siloxanes: kinetics and products of oxidation

641 by OH radicals and Cl atoms, Environ. Sci. Technol., 54, 5992−5999, 2020.

642

643 Antonelli, L., Mapelli, E., Strini, A., Cerulli, T., Leoni, R., and Stella S.: Laboratory and real scale comparative study of

644 benzyl alcohol emission from a two-component epoxy paint, Proceedings: Indoor Air, 584-589, 2002.

645

646 Atkinson, R., Aschmann, S. M., and Arey, J.: Reactions of OH and N03 Radicals with Phenol, Cresols, and 2-Nitrophenol

647 at 296 ± 2 K, Environ. Sci. Technoi. 1992, 26, 1397-1403, 1992.

648

649 Bernard, B., Magneron, I., Eyglunent, G., Daële, V., Wallington, T. J., Hurley, M. D., and Mellouki, A.: Atmospheric

650 chemistry of benzyl alcohol: kinetics and mechanism of reaction with OH radicals, Environ. Sci. Technol., 47,

651 3182−3189, 2013.

652

653 Berndt, T., Herrmann, H., Sipila, M., and Kulmala, M.: Highly oxidized second-generation products from the gas-phase

654 reaction of OH radicals with isoprene. J. Phys. Chem. A, 120 (51), 10150− 10159, 2016.

655

656 Boatright, J., Negre, F., Chen, X., Kish, C. M., Wood, B., Peel, G., Orlova, I., Gang, D., Rhodes, D., and Dudareva, N.:

657 Understanding in vivo benzenoid metabolism in petunia petal tissue, Plant Physiol., 135, 1993−2011, 2004.

658

659 Carter, W. P. L., Malkina, I. L., Cocker III, D. R., and Song, C.: Environmental chamber studies of VOC species in

660 architectural coating and mobile source emissions, South Coast Air Quality Management District Contract No. 03468,

661 2005.

662

663 Charan, S. M., Buenconsejo, R. S., and Seinfeld, J. H.: Secondary organic aerosol yields from the oxidation of benzyl

664 alcohol, Atmos. Chem. Phys., 20, 13167–13190, doi:10.5194/acp-2020-49, 2020

665

666 Charan, S. M., Huang, Y., Buenconsejo, R. S., Li, Q., Cocker III, D. R., and Seinfeld, J. H.: Secondary organic aerosol

667 formation from the oxidation of decamethylcyclopentasiloxane at atmospherically relevant OH concentrations, Atmos.

668 Chem. Phys., 22, 917-928, doi:10.5194/acp-22-917-2022, 2021.

669

670 Cheng, C. T., Chan, M. N., and Wilson, K. R.: Importance of unimolecular HO2 elimination in the heterogeneous OH

671 reaction of highly oxygenated tartaric acid aerosol, J. Phys. Chem. A, 120, 5887−5896, doi: 10.1021/acs.jpca.6b05289,

672 2016.

673

674 Coggon, M. M., Gkatzelis, G. I., McDonald, B. C., Gilman, J. B., Schwantes, R. H., Abuhassan, N., Aikin, K. C., Arendd,

675 M. F., Berkoff, T. A., Brown, S. S., Campos, T. L., Dickerson, R. R., Gronoff, G., Hurley, J. F., Isaacman-VanWertz, G.,

676 Koss, A. R., Lia, M., McKeen, S. A., Mosharyd, F., Peischl, J., Pospisilova, V., Renh, X., Wilson, A., Wu, Y., Trainer,

677 M., and Warneke, C.: Volatile chemical product emissions enhance ozone and modulate urban chemistry,

678 doi:10.1073/pnas.2026653118, PNAS, 118, 32, e2026653118, 2021.

679

680 DeBolt, S., Cook, D. R., and Ford, C. M.: L-Tartaric acid synthesis from vitamin C in higher plants, PNAS, 103 (14) 5608-

681 5613, doi: 10.1073/pnas.0510864103, 2006.

682

683 Derrien, E., Ahmar, M., Martin-Sisteron, E., Raffin, G., Queneau, Y., Marion, P., Beyerle, M., Pinel, C., and Besson, M.:

684 Oxidation of aldoses contained in softwood hemicellulose acid hydrolysates into aldaric acids under alkaline or

685   noncontrolled pH conditions, Industrial & Engineering Chemistry Research, 57 (13), 4543-4552, doi.:

686   10.1021/acs.iecr.8b00239, 2018.

687

688   Do, J. Y., Salunkhe, D. K., and Olson, L. E.: Isolation, identification and comparison of the volatiles of peach fruit as

689   related to harvest maturity and artificial ripening, J. Food Sci., 34, 618−621, 1969.

690

691   Ferri, D., Mondelli, C., Krumeich, F., and Baiker, A.: Discrimination of active palladium sites in catalytic liquid-phase

692   oxidation of benzyl alcohol, J. Phys. Chem. B., 110, 46, 22982-22986, doi:10.1021/jp065779z, 2006.

693

694   Finewax, Z., de Gow, J. A., and Ziemann, P. J.: Identification and Quantification of 4-Nitrocatechol Formed from OH

695   and NO_3 Radical-Initiated Reactions of Catechol in Air in the Presence of NO_x: Implications for Secondary Organic

696   Aerosol Formation from Biomass Burning, Environmental Science & Technology, 52 (4), 1981-1989, doi.:

697   10.1021/acs.est.7b05864, 2018.

698

699   Fu, Zi., Xie, H., Elm, J., Guo, X., Fu, Zh., and Chen, J.: Formation of low-volatile products and unexpected high

700   formaldehyde yield from the atmospheric oxidation of methylsiloxanes, Environ. Sci. Technol., 54, 12, 7136-7145,

701   doi:10.1021/acs.est.0c01090, 2020.

702

703   Gkatzelis, G. I., Coggon, M. M., McDonald, B. C., Peischl, J., Aikin, K. C., Gilman, J. B., Trainer, M., and Warneke, C.:

704   Identifying volatile chemical product tracer compounds in U.S. Cities, Environ. Sci. Technol.,

705   doi:10.1021/acs.est.0c05467, 55, 188−199, 2021.

706

707   Gowda, D., Kawamura, K., and Tachibana, E.: Identification of hydroxy- and keto-dicarboxylic acids in remote marine

708   aerosols using gas chromatography/quadruple and time-of-flight mass spectrometry, Rapid Communications in Mass

709   Spectrometry, 30(7), 992–1000, doi: 10.1002/rcm.7527, 2016.

710

711   Harrison, J. C., and Wells, J. R.: Gas-phase chemistry of benzyl alcohol: reaction rate constants and products with OH

712   radical and ozone, Atmos. Environ., 43, 798−804, 2009.

713

714 Harrison, J. C., and Wells, J. R.: 2-Butoxyethanol and benzyl alcohol reactions with the nitrate radical: rate coefficients

715 and gas-phase products, Int. J. Chem. Kinet., 44, 778−788, 2012.

716

717 Hayes, P. L., Carlton, A. G., Baker, K. R., Ahmadov, R., Washenfelder, R. A., Alvarez, S., Rappenglück, B., Gilman, J.

718 B., Kuster, W. C., de Gouw, J. A., Zotter, P., Prévôt, A. S. H., Szidat, S., Kleindienst, T. E., Offenberg, J. H., Ma, P. K.,

719 and Jimenez, J. L.: Modeling the formation and aging of secondary organic aerosols in Los Angeles during CalNex 2010,

720 Atmos. Chem. Phys., 15, 5773–5801, 2015.

721

722 Hinton, M. R.: Xylaric acid, D-arabinaric acid (D-lyxaric acid), L-arabinaric acid (L-lyxaric acid), and Ribaric acid-1,4-

723 lactone; Synthesis and isolation-synthesis of polyhydroxypolyamides therefrom, Theses, Dissertations, & Professional

724 Papers. 1202, https://scholarworks.umt.edu/etd/1202, 2008.

725

726 Hodzic, A., Jimenez, J. L., Madronich, S., Aiken, A. C., Bessagnet, B., Curci, G., Fast, J., Lamarque, J.-F., Onasch, T.

727 B., Roux, G., Schauer, J. J., Stone, E. A., and Ulbrich, I. M.: Modeling organic aerosols during MILAGRO: importance

728 of biogenic secondary organic aerosols, Atmos. Chem. Phys., 9, 6949–6981, 2009.

729

730 Horvat, R. J., Chapman, G. W., Jr., Robertson, J. A., Meredith, F. I., Scorza, R., Callahan, A. M., and Morgens, P.:

731 Comparison of the volatile compounds from several commercial peach cultivars, J. Agric. Food Chem., 38, 234−237,

732 1990.

733

734 Humes, M. B., Wang, M., Kim, S., Machesky, J. E., Gentner, D. R., Robinson, A. L., Donahue, N. M., and Presto, A. A.:

735 Limited secondary organic aerosol production from acyclic oxygenated volatile chemical products, Environ. Sci. Technol.

736 56, 4806−4815, 2022.

737

738 Humpf, H. U., and Schreier, P.: Bound aroma compounds from the fruit and the leaves of blackberry (Rubus laciniata L.),

739 J. Agric. Food Chem., 39, 1830−1832, 1991.

740

741 Ikemori, E., Nakayama, T., and Hasegawa, H.: Characterization and possible sources of nitrated mono- and di-aromatic

742 hydrocarbons containing hydroxyl and/or carboxyl functional groups in ambient particles in Nagoya, Japan, Atmos.

743 Environ., 211, 91-102, 2019.

744

745 Janechek, N. J., Marek, R. F., Bryngelson, N., Singh, A., Bullard, R. L., Brune, W. H., and Stanier, C. O.: Physical

746 properties of secondary photochemical aerosol from OH oxidation of a cyclic siloxane, Atmos. Chem. Phys., 19, 1649–

747 1664, 2019.

748

749 Jaoui, M., and Kamens, R. M.: Mass balance of gaseous and particulate products analysis from α-pinene/NO$_x$/air in the

750 presence of natural sunlight, J. Geophys. Res., 106, D12, 12,541-12,558, doi:10.1029/2001JD900005, 2001.

751

752 Jaoui, M., Kleindienst, T. E., Lewandowski, M., and Edney, E. O.: Identification and quantification of aerosol polar

753 oxygenated compounds bearing carboxylic and/or hydroxyl groups, 1. Method development, Anal. Chem., 76, 4765–

754 4778, 2004.

755

756 Jaoui, M., Kleindienst, T. E., Lewandowski, M., Offenberg, J. H., and Edney, E. O.: Identification and quantification of

757 aerosol polar oxygenated compounds bearing carboxylic or hydroxyl groups. 2. Organic tracer compounds from

758 monoterpenes, Environ. Sci. Technol., 39, 5661–5673, 2005.

759

760 Jaoui, M., Kleindienst, T. E., Docherty, K. S., Lewandowski, M., and Offenberg, J. H.: Secondary organic aerosol

761 formation from the oxidation of a series of sesquiterpenes: a-cedrene, b-caryophyllene, a-humulene and a-farnesene with

762 O$_3$, OH and NO$_3$ radicals, Environ. Chem. 10, 178–193, doi:10.1071/EN13025, 2013.

763

764 Jaoui, M., Lewandowski, M., Docherty, K., Offenberg, J. H., and Kleindienst, T. E.: Atmospheric oxidation of 1,3-

765 butadiene: characterization of gas and aerosol reaction products and implications for PM$_{2.5}$, Atmos. Chem. Phys., 13681–

766 13704, doi: 10.5194/acp-14-1368114, 2014.

767

768 Jaoui, M., Lewandowski, M., Offenberg, H. J., Colon, M., Docherty, K. S., and Kleindienst, T. E: Characterization of

769 aerosol nitroaromatic compounds: Validation of an experimental method, Mass Spectrom., 53, 680–692, 2018.

770

771 Jaoui, M., Szmigielski, R., Nestorowicz, K., Kolodziejczyk, A., Sarang, K., Rudzinski, K. J., Konopka, A., Bulska, E,

772 Lewandowski, M., And Kleindienst, T. E.: Organic hydroxy acids as highly oxygenated molecular (HOM) tracers for

773 aged isoprene aerosol, Environmental Science & Technology, 53 (24), 14516-14527, doi: 10.1021/acs.est.9b05075, 2019.

774

775 Jaoui, M., Piletic, I., Szmigielski, R., Rudzinski, J. K., E, Lewandowski, M., Riedel, T. P., and Kleindienst, T. E.: Rapid

776 production of highly oxidized molecules in isoprene aerosol via peroxy and alkoxy radical isomerization pathways in low

777 and high NO_x environments: Combined laboratory, computational and field studies, Science of The Total Environment,

778 775, 145592, doi: 10.1016/j.scitotenv.2021.145592, 2021

779

780 Jenkin, M. E., Saunders, S. M., Wagner, V., and Pilling, M. J.: Protocol for the development of the Master Chemical

781 Mechanism, MCM v3 (Part B): tropospheric degradation of aromatic volatile organic compounds, Atmos. Chem. Phys.,

782 3, 181–193, https://doi.org/10.5194/acp-3-181-2003, 2003.

783

784 Khare, P., and Gentner, D. R.: Considering the future of anthropogenic gas-phase organic compound emissions and the

785 increasing influence of non-combustion sources on urban air quality, Atmos. Chem. Phys., 18, 5391–5413, 2018.

786

787 Kleindienst, T. E., Edney, E. O., Lewandowski, M., Offenberg, J. H., and Jaoui M.: Secondary organic carbon and aerosol

788 yields from the irradiations of isoprene and $\square$-pinene in the presence of NO_x and SO_2, Environ. Sci. Technol., 40, 3807–

789 3812, 2006.

790

791 Kleindienst, T. E., Lewandowski, M., Offenberg, J. H., Jaoui, M., and Edney, E. O.: The formation of secondary organic

792 aerosol from the isoprene + OH reaction in the absence of NO_x, Atmos. Chem. Phys., 9, 6541–6558, 2009.

793

794   Kleindienst, T. E., Jaoui, M., Lewandowski, M., Offenberg, J. H., and Docherty, K. S.: The formation of SOA and

795   chemical tracer compounds from the photooxidation of naphthalene and its methyl analogs in the presence and absence

796   of nitrogen oxides, Atmos. Chem. Phys., doi:10.5194/acp-12-8711-2012, 12, 8711–8726, 2012.

797

798   Kroflic, A., Hus, M., Grilc, M., and Grgic, I.: Underappreciated and complex role of nitrous acid in aromatic nitration

799   under mild environmental conditions: the case of activated methoxyphenols, Environ. Sci. Technol., 52, 13756–13765,

800   https://doi.org/10.1021/acs.est.8b01903, 2018.

801

802   Kroll, J. H., Chan, A. W. H., Ng, N. L., Flagan, R. C., and Seinfeld, J. H.: Reactions of semivolatile organics and their

803   effects on secondary organic aerosol formation, Environ. Sci. Technol., 41, 3545–3550, 2007.

804

805   Larsen, M., and Poll, L.: Odor thresholds of some important aroma compounds in raspberries, Z. Lebensm. Unters. Forsch,

806   191, 129−131, 1990.

807

808   Lewandowski, M., Jaoui, M., Offenberg, J. H., Krug, J. D., and Kleindienst, T. E.: Atmospheric oxidation of isoprene and

809   1,3-butadiene: influence of aerosol acidity and relative humidity on secondary organic aerosol, Atmos. Chem. Phys., 15,

810   3773–3783, doi:10.5194/acp-15-3773-2015, 2015.

811

812   Li, W., Li, L., Chen, C-L, Kacarab, M., Peng, W., Price, D., Xu, J., and Cocker III, D. R.: Potential of select intermediate-

813   volatility organic compounds and consumer products for secondary organic aerosol and ozone formation under relevant

814   urban conditions, Atmos. Environ., 118, 109-117, 2018.

815

816   Lu, Q., Murphy, B. N., Momei Q., Adams, P. J., Zhao, Y., Pye, H. O. T., Efstathiou, C., Allen, C., and Robinson, A. L.:

817   Simulation of organic aerosol formation during the CalNex study: updated mobile emissions and secondary organic

818   aerosol parameterization for intermediate-volatility organic compounds, Atmos. Chem. Phys., 20, 4313–4332, 2020.

819

820   McDonald, B. C., De Gouw, J. A., Gilman, J. B., Jathar, S. H., Akherati, A., Cappa, C. D., Jimenez, J. L., Lee-Taylor, J.,

821   Hayes, P. L., McKeen, S. A., Cui, Y. Y., Kim, S. W., Gentner, D. R., Isaacman-VanWertz, G., Goldstein, A. H., Harley,

822 R. A., Frost, G. J., Roberts, J. M., Ryerson, T. B., and Trainer, M.: Volatile chemical products emerging as largest

823 petrochemical source of urban organic emissions, Science, 359, 760–764, 2018.

824

825 Milani, A., Al-Naiema, I. M., and Stone, E. A: Detection of a secondary organic aerosol tracer derived from personal care

826 products, Atmos. Environ., 246, 118078, 2021.

827

828 Mohr, C., DeCarlo, P. F., Heringa, M. F., Chirico, R., Richter, R., Crippa, M., Querol, X., Baltensperger, U., and Prévôt,

829 A. S. H.: Spatial variation of aerosol chemical composition and organic components identified by positive matrix

830 factorization in the Barcelona region, Environ. Sci. Technol., 49, 10421–10430, 2015.

831

832 Namysl, S., Pelucchi, M., Maffei, L. P., Herbinet, O., Stagni, A., Faravelli, T., and Battin-Leclerc, F.: Experimental and

833 modeling study of benzaldehyde oxidation, Combustion and Flame, 211, 124–132, 2020.

834

835 Offenberg, J. H., Lewandowski, M., Edney, E. O., Kleindienst, T. E., Jaoui, M.: Investigation of a systematic offset in the

836 measurement of organic carbon with a semicontinuous analyzer, J. A&WMA, 57:5, 596-599, doi:10.3155/1047-

837 3289.57.5.596, 2007

838

839 Orlova, I., Marshall-Colón, A., Schnepp, J., Wood, B., Varbanova, M., Fridman, E., Blakeslee, J. J., Peer, W. A., Murphy,

840 A. S., Rhodes, D., Pichersky, E., and Dudareva, N.: Reduction of Benzenoid synthesis in petunia flowers reveals multiple

841 pathways to benzoic acid and enhancement in auxin transport, Plant Cell, 18, 3458−3475, 2006.

842

843 Pennington, E. A., Seltzer, K. M., Murphy, B. N., Qin, M., Seinfeld, J. H., Pye, H. O. T.: Modeling secondary organic

844 aerosol formation from volatile chemical products, Atmos. Chem. Phys., doi:10.5194/acp-21-18247-18261-2021, 18247-

845 18261, 2021.

846

847 Piletic, I. R., and Kleindienst, T. E.: Rates and Yields of Unimolecular Reactions Producing Highly Oxidized Peroxy

848 Radicals in the OH-Induced Autoxidation of α-Pinene, β-Pinene, and Limonene, *The Journal of Physical Chemistry A.*

849 *126* (1), 88-100, doi: 10.1021/acs.jpca.1c07961, 2022.

850

851   Qin, M. M., Murphy, B. N., Isaacs, K. K., McDonald, B. C., Lu, Q. Y., McKeen, S. A., Koval, L., Robinson, A. L.,

852   Efstathiou, C., Allen, C., and Pye, H. O. T.: Criteria pollutant impacts of volatile chemical products informed by near-

853   field modelling, Nature Sustainability, 4, 129–137, https://doi.org/10.1038/s41893-020-00614-1, 2021.

854

855   Rohl, A., and Lammedl. G.: Determination of malic acid and other C4 dicarboxylic acids in atmospheric aerosol samples,

856   Chemosphere, 46(8), 1195-1199, doi: 10.1016/s0045-6535(01)00243-0, 2002.

857

858   Sankar, S., Nowicka, E., Carter, E., Murphy, D. M., Knight, D. W., Bethell, D., and Hutchings, G. J.: The benzaldehyde

859   oxidation paradox explained by the interception of peroxy radical by benzyl alcohol, Nature Communic,

860   doi:10.1038/ncomms4332, 5, 3332, 2014.

861

862   Seltzer, K. M., Murphy, B. N., Pennington, E. A., Allen, C., Talgo, K., and Pye, H. O. T.: Volatile chemical product

863   enhancements to criteria pollutants in the United States, Environ. Sci. technol., doi:10.1021/acs.est.1c04298, 2021.

864

865   Shilling, J. E., Chen, Q., King, S. M., Rosenoern, T., Kroll, J. H., Worsnop, D. R., McKinney, K. A., and Martin, S. T.:

866   Particle mass yield in secondary organic aerosol formed by the dark ozonolysis of α-pinene, Atmos. Chem. Phys., 8,

867   2073–2088, doi:10.5194/acp-8-2073-2008, 2008.

868

869   Smith, D. F., Kleindienst, T. E., and Hudgens, E. E.: Improved high-performance liquid chromatographic method for

870   artifact free measurements of aldehydes in the presence of ozone using 2,4-dinitrophenylhydrazine, J. Chromatogr. A,

871   483, 431–436, 1989.

872

873   Stockwell, C. E., Coggon, M. M., Gkatzelis, G. A., Ortega, J., McDonald, B. C., Peischl, J., Aikin, K., Gilman, J. B.,

874   Trainer, M., and Warneke, C.: Volatile organic compound emissions from solvent- and water borne coatings:

875   compositional differences and tracer compound identifications, Atmos. Chem. Phys., 21, 6005–6022, doi:10.5194/acp-

876   21-6005-2021, 2021.

877

878   Urakami, K., Kobayashi, C., Miyazaki, Y., Nishijima, K., and Yoshimura, Y.: Degradation products generated by

879   sonication of benzyl alcohol, a sample preparation solvent for the determination of residual solvents in pharmaceutical

880   bulks, on capillary gas chromatography, Chem. Pharm. Bull., 48, 1299–1303, 2000.

881

882   Vallat, A., and Dorn, S.: Changes in volatile emissions from apple trees and associated response of adult female codling

883   moths over the fruit-growing season, J. Agric. Food Chem., 53, 4083−4090, 2005.

884

885   Vidovic, K., Lasic Jurkovic, D., Sala, M., Kroflic, A., and Grgic, I.: Nighttime aqueous-phase formation of nitrocatechols

886   in the atmospheric condensed phase, Environ. Sci. Technol., 52, 9722– 9730, https://doi.org/10.1021/acs.est.8b01161,

887   2018.

888

889   Vlachou, A., Daellenbach, K. R., Bozzetti, C., Chazeau, B., Salazar, G. A., Szidat, S., Jaffrezo, J. L., Hueglin, C.,

890   Baltensperger, U., El Haddad, I., and Prévôt, A. S.: Advanced source apportionment of carbonaceous aerosols by coupling

891   offline AMS and radiocarbon size-segregated measurements over a nearly 2-year period. Atmos. Chem. Phys., 18, 6187–

892   6206, 2018.

893

894   Wang, L.: The atmospheric oxidation mechanism of benzyl alcohol initiated by OH radicals: the addition channels, Chem.

895   Phys. Chem., *16* (7), 1542-1550, doi:10.1002/cphc.201500012, 2015.

896

897   Wang, N., Jorga, S. D., Pierce, J. R., Donahue, N. M., and Pandis, S. N.: Particle wall-loss correction methods in smog

898   chamber experiments, Atmos. Meas. Tech., 11, 6577–6588, doi:10.5194/amt-11-6577-2018, 2018.

899

900   Wang, Y., Hu, M., Wang, Y., Zheng, J., Shang, D., Yang, Y., Liu, Y., Li, X., Tang, R., Zhu, W., Du, Z., Wu, Y., Guo, S.,

901   Wu, Z., Lou, S., Hallquist, M., and Yu, J. Z.: The formation of nitro-aromatic compounds under high NOx and

902   anthropogenic VOC conditions in urban Beijing, China, Atmos. Chem. Phys., 19, 7649–7665, 2019.

903

904   Weschler, C. J.: Chemistry in indoor environments: 20   years of research, Indoor Air, 21 (3), 205-218, 2011.

905

906 Wu, Y., and Johnston, M. V.: Molecular characterization of secondary aerosol from oxidation of cyclic methylsiloxanes,

907 J. Am. Soc. Mass. Spectr., 27, 402–409, doi:10.1007/s13361-015-1300-1, 2016.

908

909 Wu, Y., and Johnston, M. V.: Aerosol formation from OH oxidation of the volatile cyclic methyl siloxane (cVMS)

910 Decamethylcyclopentasiloxane, Environ. Sci. Technol., 51, 4445– 4451, doi:10.1021/acs.est.7b00655, 2017.

911

912 Zhao, B., Wang, S., Donahue, N. M., Jathar, S. H., Huang, X., Wu, W., Hao, J., and Robinson, A. L.: Quantifying the

913 effect of organic aerosol aging and intermediate volatility emissions on regional-scale aerosol pollution in China, Sci.

914 Rep., 6, 28815, doi:10.1038/srep28815, 2016.

915

916 Zhang, X., Cappa, C. D., Jathar, S. H., McVay, R. C., Ensberg, J. J., Kleeman, M. J., and Seinfeld, J. H.: Influence of

917 vapor wall loss in laboratory chambers on yields of secondary organic aerosol, PNAS, doi:10.1073/pnas.1404727111,

918 111 (16), 5802-5807, 2014.

919

920

921

922

923

924

925

926

927

928

929

930

931

932

933

934 **Table 1.** Initial conditions for BnOH experiments in the presence and absence of NO.

Exp. IDs	BnOH (ppb)	H$_2$O$_2$ (ppm)	NO[a] (ppb)	Seed surface area (nm^2 cm^{-3})	BnOH/NO (ppb/ppb)	T (^{o}C)	RH (%)
ER-889	385	-	178	4.67 x 10^7	2.2	24.5	31.0
ER-890	355	-	96	4.94 x 10^7	3.7	24.5	31.1
ER-891	723	-	188	9.88 x 10^7	3.8	24.6	31.3
ER-892	319	3.04	-	1.36 x 10^6	-	25.7	< 4.0

935 T: temperature; RH: relative humidity. Seed aerosol at 1 µg m^{-3}. [a]: The initial NOx during the irradiations was greater than 98% NO.

936

937 **Table 2.** Steady-state GP and reacted BnOH and NO concentration during the irradiations.

Exp. IDs	NO (ppb)	Reacted NO (ppb)	BnOH (ppb)	Reacted BnOH (ppb)	BnOH/NO ratio (ppb/ppb)	O$_3$ (ppb)	NOy (ppb)
ER889	78	100	132	253	1.7	30	163
ER890	9	87	132	223	14.7	147	80
ER891	29	159	387	336	13.4	11	146
ER892	-	-	85	234	-	28	-

938

939 **Table 3.** Formation and yields of SOA (Y$_{SOA}$) and SOC (Y$_{SOC}$). All organic and carbon aerosol masses are corrected for

940 a wall loss of 0.067 h^{-1} (Kleindienst et al., 2012).

Exp. IDs	SOA (µg/m^3)	SOC (µgC/m^3)	SOA/SOC	Y$_{SOA}$ (%)	Y$_{SOC}$ (%)
ER889	39.6	23.2	1.7	3.6	2.7
ER890	56.1	30.3	1.9	5.7	4.0
ER891	119.5	58.9	2.0	8.1	5.1
ER892	52.9	24.8	2.1	5.2	3.1

941
942
943
944
945
946
947
948
949
950
951

952 **Table 4.** Steady state carbonyl concentrations (ppmV) during BnOH oxidation (FH: formaldehyde; AH: acetaldehyde;

953 Ac: acetone; MA: methacrolein; BN: 2-butanone; BnAld: benzaldehyde; G: glyoxal; MG: methylglyoxal).

Exp. ID	FH	AH	Ac	MA	BN	BnAld	G	MG
ER889	2.4	1.2	1.0	1.0	0.6	23.09	5.0	0.6
ER890	1.5	2.8	-	-	2.9	18.2	3.8	0.4
ER891	5.1	2.5	1.3	2.0	1.4	30.8	8.6	0.6
ER892	181.7	23.5	-	0.8	0.8	5.2	7.8	1.6

954

955

956

957

958

959

960

961

962

963

964

965

966

967

968

969

970

971
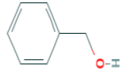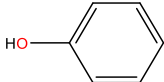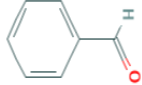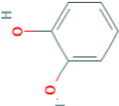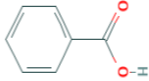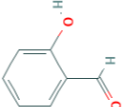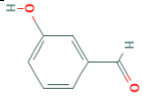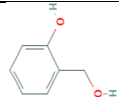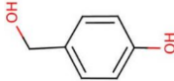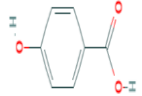
972

973

974

975

976 **Table 5.** Summary of selected reaction products detected and identified either in gas-phase (GP), particle phase (PP) or

977 both from BnOH/NOx, and BnOH/H_2O_2 experiments. Tables 6 and 7 shows additional aerosol species with high oxygen

978 to carbon ratio and/or nitro group. NA: not applicable. [a]: underivatized m/z are given. *: identified with authentic standard.

IUPAC/common nomenclature	Formula	m/z BSTFA (EI)	MW [MW$_{BSTFA}$] (g mol^{-1})	Proposed Structure	Detected
Benzyl alcohol (BnOH)	C_7H_8O	165, 91, 135, 180, 73	108 [180]		GP
Phenol	C_6H_6O	73, 151, 166, 94, 65	94 (166)		GP, PP
Benzaldehyde (BnAld)	C_7H_6O	106, 105, 77, 77, 51	106 (NA)		GP, PP
Benzene-1,2-diol (catechol)	$C_6H_6O_2$	239, 255, 80, 283, 73	110 (254)		PP
Benzoic acid	$C_7H_6O_2$	179, 105, 135, 77, 194	122 (194)		GP, PP
Salicylaldehdye	$C_7H_6O_2$	179, 105, 135, 77, 194	122 (194)		GP
3-Hydroxy benzaldehyde	$C_7H_6O_2$	179, 105, 135, 77, 194	122 (194)		GP
2-Hydroxybenzyl alcohol (salicyl alcohol)	$C_7H_8O_2$	73, 253, 179, 268, 147	124 (268)		GP, PP
4-Hydroxybenzyl alcohol	$C_7H_8O_2$	73, 179, 253, 268, 147	124 (268)		GP, PP
4-Hydroxybenzoic acid (*p*-salicylic acid)	$C_7H_6O_3$	267, 223, 193, 282, 73	138 (282)		PP [H_2O_2]
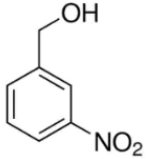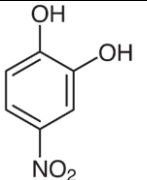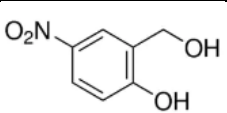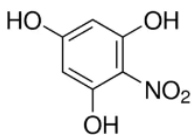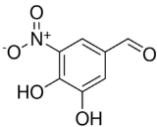
979

980 **Table 6.** Highly oxygenated products (O:C > 1.3) identified in benzyl alcohol photooxidation in the presence of NOx, or
981 H_2O_2. *: identified with authentic standard. *L*-Tartaric acid and *D*-tartaric acid co-elute. The structure of 4-oxo-D-arabonic
982 acid isomer and 2,3,5-Trihydroxy-4-oxopentanal isomer are shown for trihydroxy-oxo-pentanoic acid, and trihydroxy-
983 oxo-pentanal, respectively. Four peaks with similar fragments/adducts as pentaric acid were observed.

Nomenclature	Chemical Formulae	O/C Ratio (by wt)	*m/z* BSTFA Derivative (CI-CH4); (EI)	MW (MW$_{BSTFA}$)	Proposed Structure
Epoxysuccinic acid (2 peaks)	$C_4H_4O_5$	1.7	187, 261, 73, 277, 173 73, 173, 261, 129, 143	132 (276)	
2-Hydroxybutanedioic acid* (malic acid)	$C_4H_6O_5$	1.7	233, 335, 73, 307, 351 73, 147, 233, 245, 335	134 (350)	
Trihydroxy-oxo-pentanal (5 peaks)	$C_5H_8O_5$	1.3	73, 275, 203, 349, 393 147, 73, 349, 233, 259	148 (364)	
meso-Tartaric acid*	$C_4H_6O_6$	2.0	423, 321, 277, 439, 73 73, 147, 292, 219, 423	150 (438)	
L-Tartaric acid*	$C_4H_6O_6$	2.0	423, 321, 277, 439, 73 73, 147, 292, 219, 423	150 (438)	
Trihydroxy-oxo-pentanoic acid (8 peaks)	$C_5H_8O_6$	1.6	73, 437, 363, 481, 493 217, 73, 147, 437, 292	164 (452)	
D-Arabinonic acid* (Arabic acid)	$C_5H_{10}O_6$	1.6	361, 217, 73, 435, 525 204, 437, 73, 147, 319	166 (526)	
Pentaric acid* (4 peaks)	$C_5H_8O_7$	1.9	525, 333, 407, 435, 73 73, 292, 189, 407, 525	180 (540)	

984
985
986
987

988   **Table 7.** NACs identified in benzyl alcohol photooxidation in the presence of NOx.

Nomenclature	Chemical Formula Rt (min)	*m/z* BSTFA Derivative (CH$_4$-CI) (EI)	MW (MW$_{bstfa}$)	Observed in GP; PP [GP/PP ratio]	Proposed Structure
3-nitrobenzyl alcohol[a]	C$_7$H$_7$NO$_3$ (25.93)	226, 210, 180, 136, 73 210, 180, 165, 194, 73	153 (225)	PP, GP [1.71]	
4-nitrocatechol[a]	C$_6$H$_5$NO$_4$ (30.86)	300, 284, 328, 254, 73 73, 284, 299, 269, 223	155 (299)	PP, GP [0.08]	
2-hydroxy-5-nitro benzyl alcohol[a] (4 isomers)	C$_7$H$_7$NO$_4$ (34.26)	314, 298, 268, 342, 73 298, 283, 191, 314, 73	169 (313)	PP, GP [0.08]	
2-nitro phloroglucinol[a] (4 isomers)[b]	C$_6$H$_5$NO$_5$ (35.62)	388, 372, 416, 428, 73 73, 372, 387, 284, 306	171 (387)	PP	
3,4-dihydroxy-5-nitrobenzyl alcohol (4 isomers)[c]	C$_7$H$_7$NO$_5$ (38.18)	388, 372, 416, 428, 73 73, 224, 3876, 401, 356	185 (401)	PP	

989   [a]: identified using authentic standards. [b]: Three additional peaks eluted at 33.76, 34.70, 34.76 min with similar mass spectra
990   as those recorded for 2-nitrophloroglucinol standard were detetcted, and the structure given here is for 2-
991   nitrophloroglucinol. [c]: Three additional peaks eluted at 35.94, 36.60, 38.18 min with similar mass spectra were detetcted.

992
993
994
995
996
997
998
999
1000
1001
1002

1003
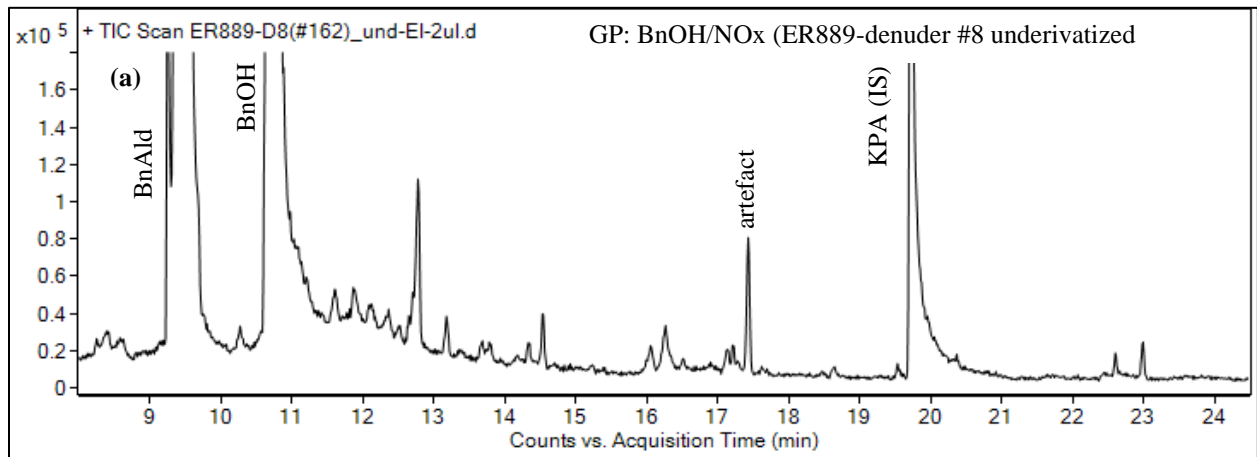
1004
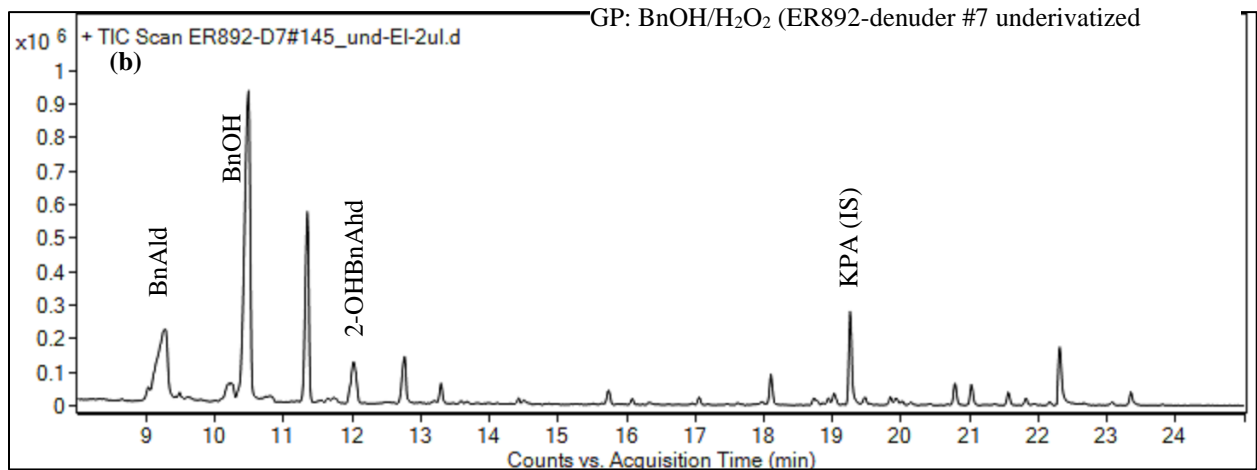
1005
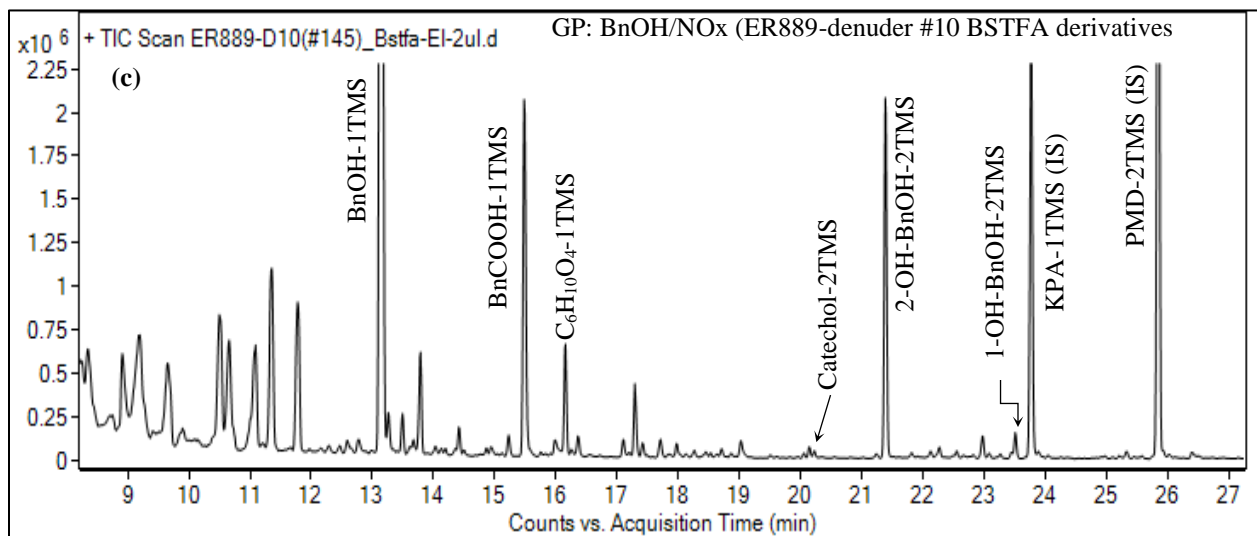
1006 **Figure 1.** Portion of GC-MS total ion chromatogram in EI mode of GP underivatized denuder extract (a) ER-889 (presence of NOx),

1007 (b) ER-892 (absence of NOx), and (c) ER889- (presence of Nox) as BSTFA derivatives.
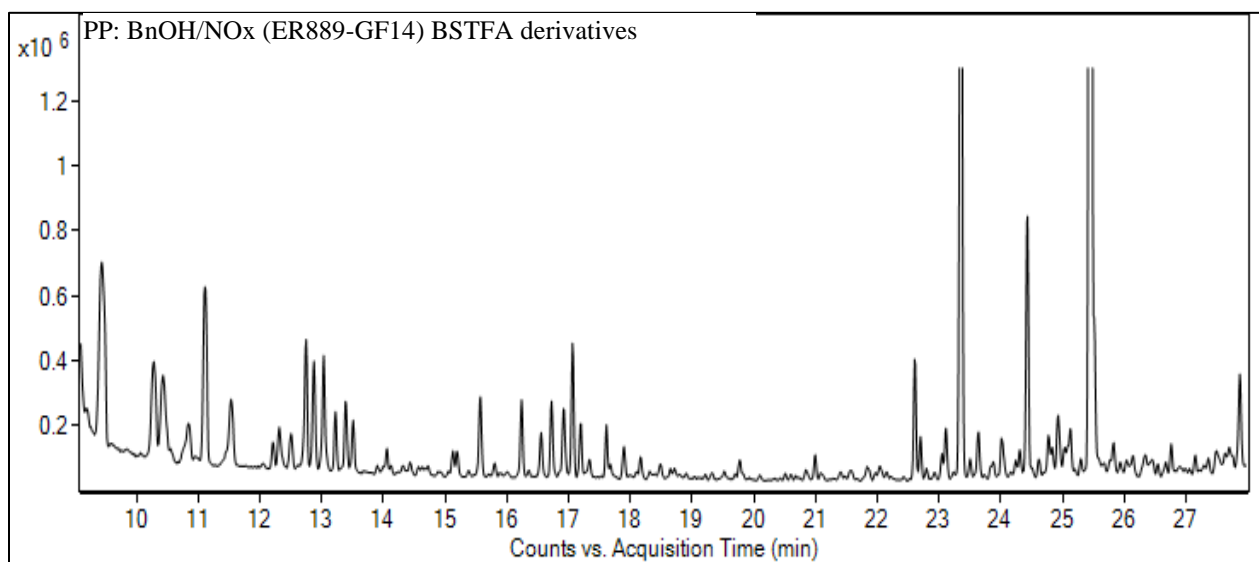
1008
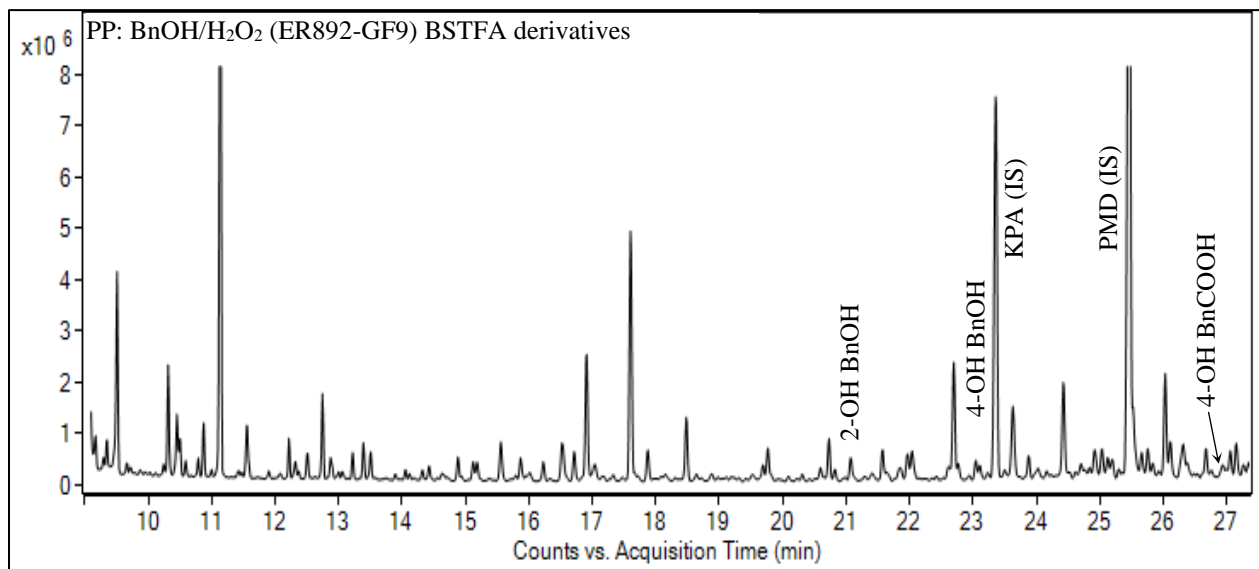
1009
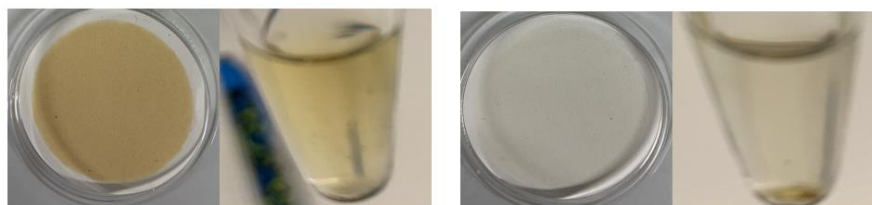
1010 **F1**: BnOH/NOx   **E1**: methanol extract   **F2**: BnOH/H2O2   **E2**: methanol extract

1011 **Figure 2.** Portion of GC-MS total ion chromatograms (EI mode) of particle-phase extracts: (top) BSTFA derivatized sample form ER-

1012 889 (presence of NOx), (middle) BSTFA derivatives from ER-892 (absence of NOx), (bottom) effect of mixture changes in filter and

1013 methanol extract appearance: BnOH/NOx filter (F1); BnOH/H2O2 (F2). The same volume of air was sampled on each filter.
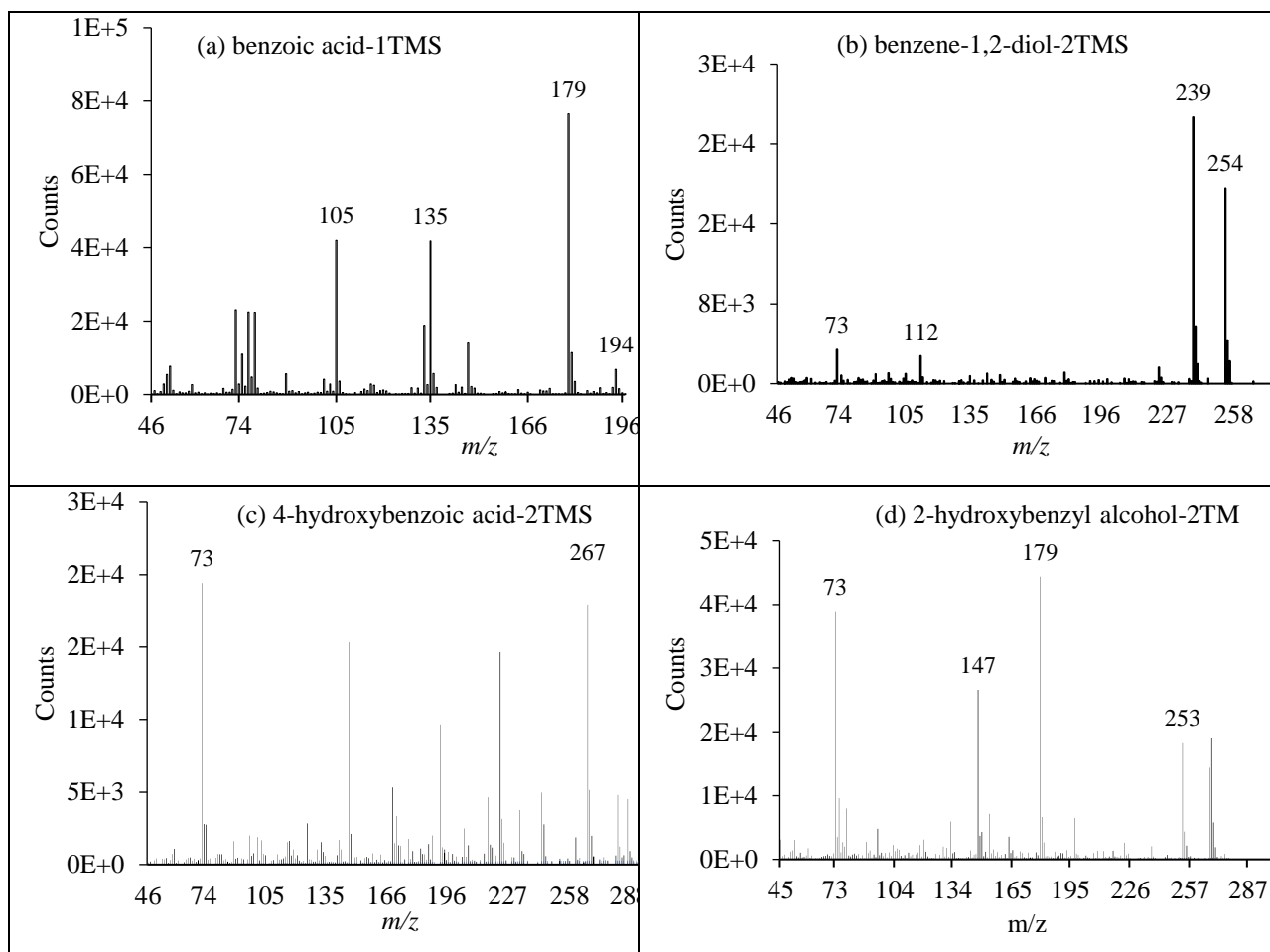
Figure 3. Positive EI mass spectra of BSTFA derivatives of selected ring-containing products: benzoic acid, benzene-1,2-diol, 4-hydroxybenzoic acid; and 2-hydroxybenzyl alcohol.
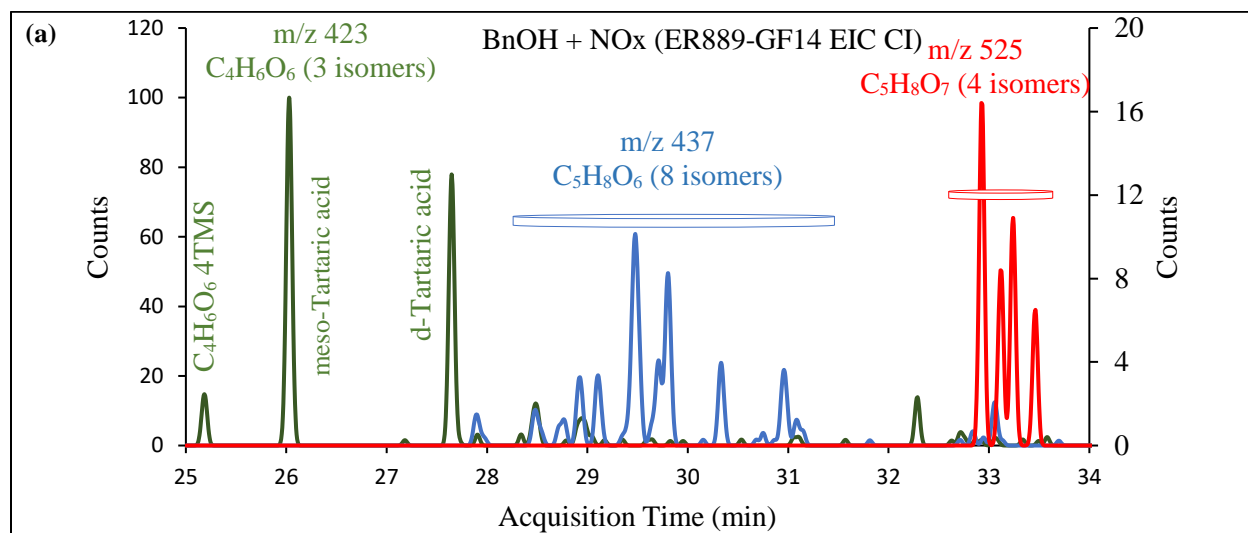
1021
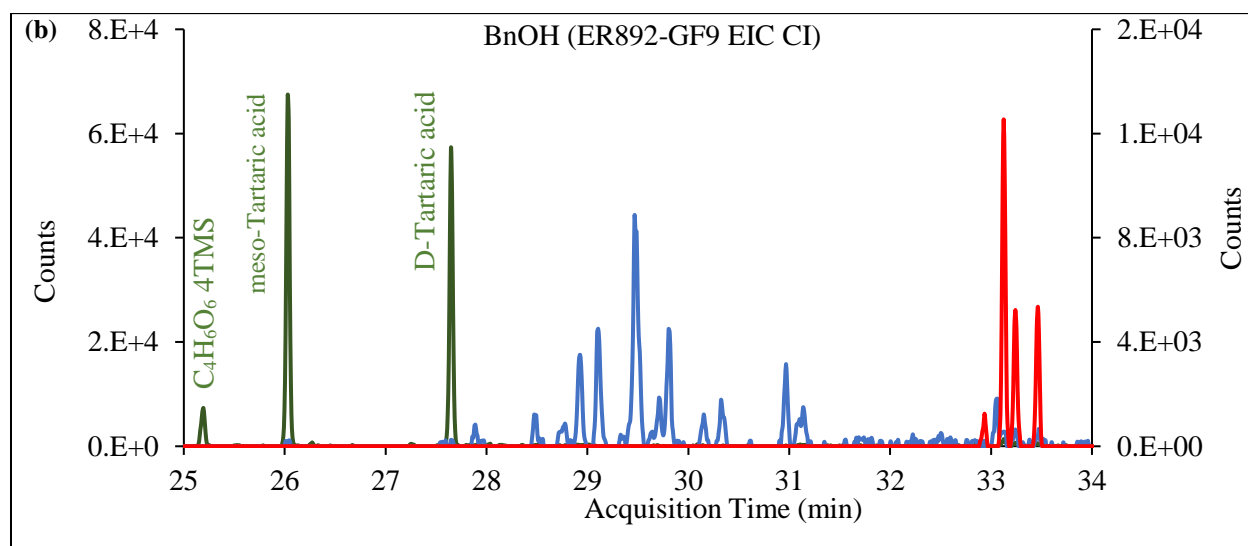
1022
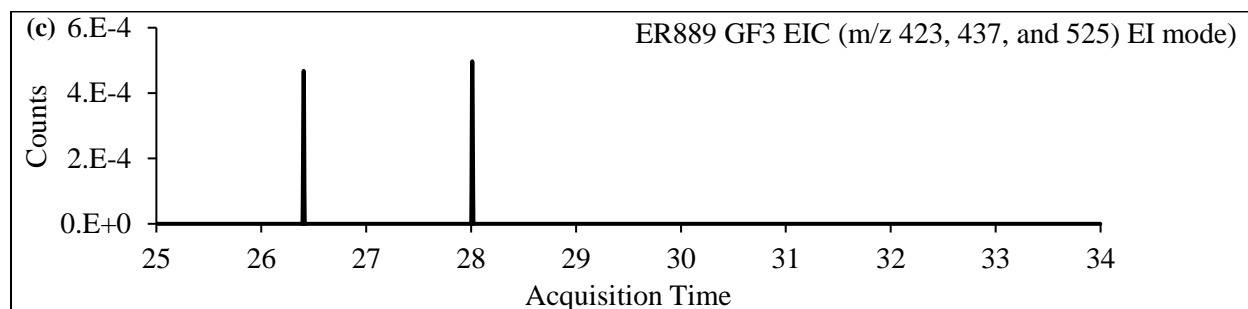
1023

1024 **Figure 4.** Portion (25-34 min) of GC-MS extracted ion chromatograms (CI-CH$_4$) at *m/z* 423 (green); m/z 437 (blue); and m/z 525 (red)

1025 merged in one chromatogram (a) BnOH in the presence of NOx; (b) BnOH in the presence of H$_2$O$_2$ and absence of NOx; (c) Chamber

1026 background. Red and top blue: right axis.
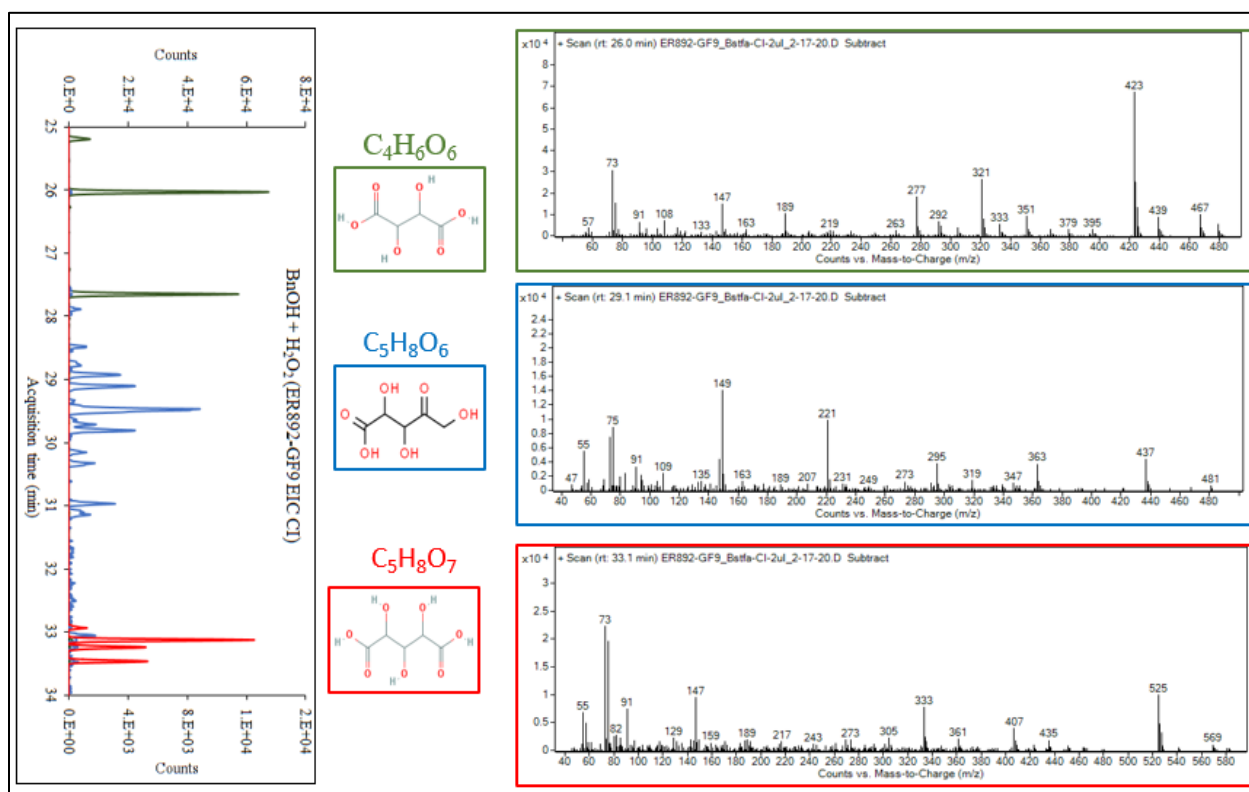
Figure 5. Mass spectra (methane-CI) of ester TMS derivatives of meso-tartaric acid (top right), trihydroxy-oxo-pentanoic acid (middle right), (c) pentaric acid (bottom right), along with the portion of GC-MS extracted ion chromatograms shown in figure 6. Chemical formulae and chemical structure associated with each group is given in the middle column.
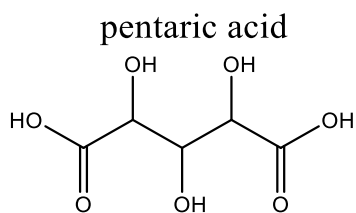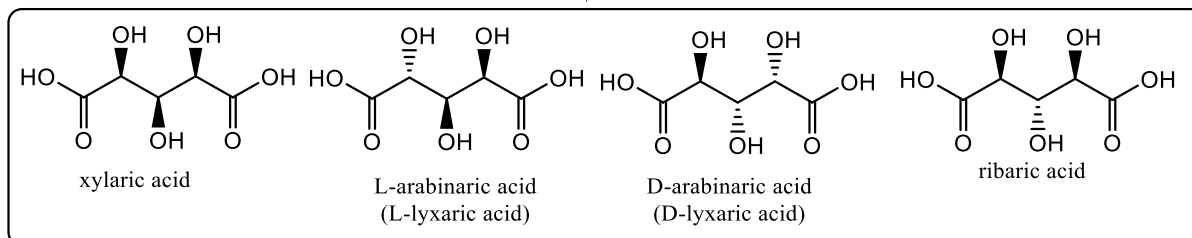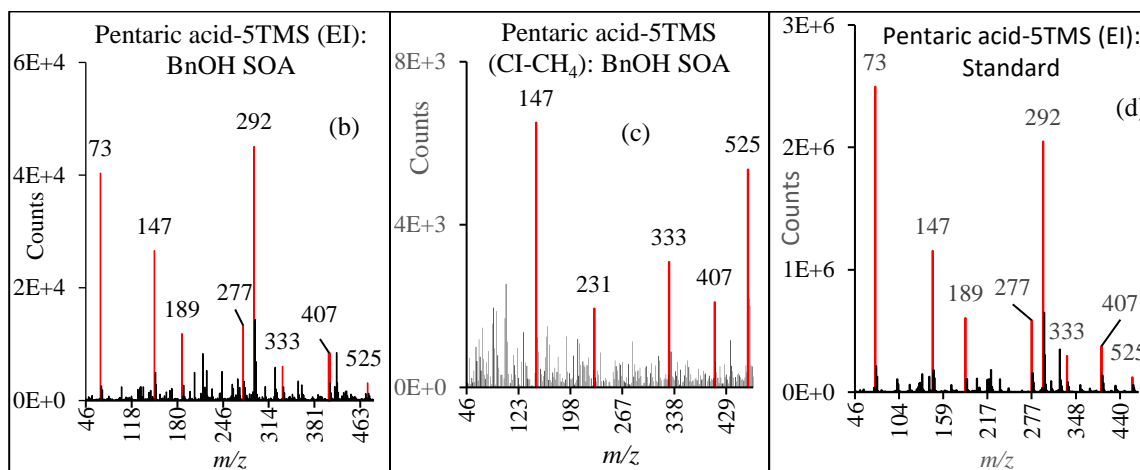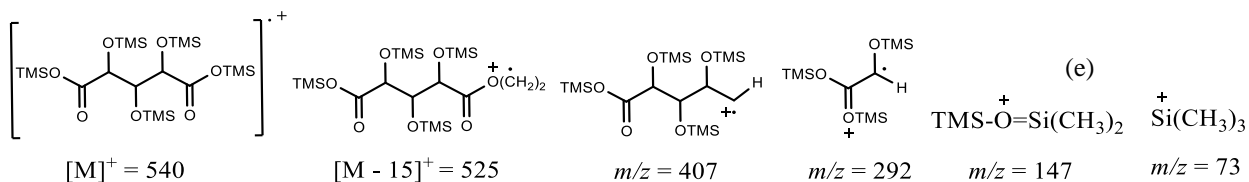
Figure 6. Molecular structures of pentaric acid and its isomers (a); mass spectra of TMS derivatives of pentaric acid acquired for smog chamber SOA (EI: b, CI: c) and authentic standard (d: EI); Major pentaric acid fragments observed in EI mode (e).
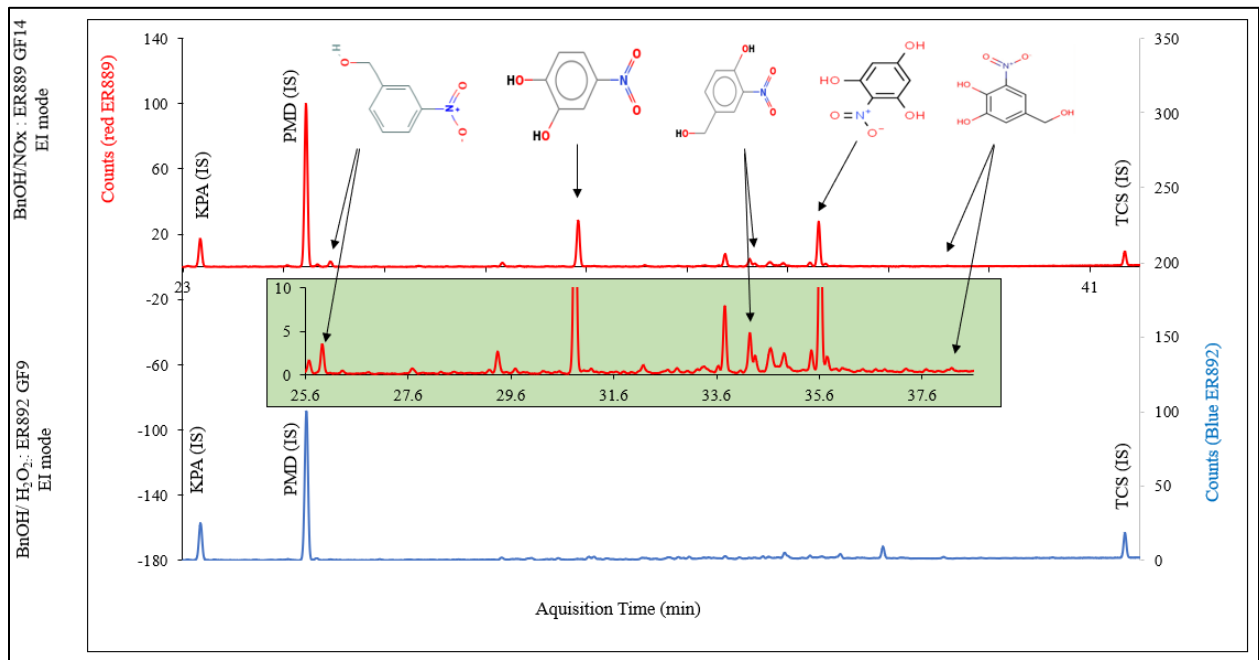
1050

1051 **Figure 7.** Portion of GC-MS extracted ion chromatograms (EI mode) at *m/z* 210, 165 (IS), 299 (IS), 300, 298, 372, 388 associated with

1052 nitroaromatic compounds merged in one chromatogram (red) BnOH in the presence of NOx (ER889); (blue) BnOH in the presence of

1053 H_2O_2 and absence of NOx (ER892).

1054

1055

1056

1057

1058